REPORT DOCUMENTATION PAGE

Form Approved
OMB No. 0704-0188

1. AGENCY USE ONLY (Leave blank)	2. REPORT DATE	3. REPORT TYPE AND DATES COVERED
	April 1995	Final Report

4. TITLE AND SUBTITLE

Shock Propagation in Crustal Rock

5. FUNDING NUMBERS

Contract
F49620-92-J-0402

6. AUTHOR(S)

Thomas J. Ahrens
William W. Anderson
Yusheng Zhao

7. PERFORMING ORGANIZATION NAME(S) AND ADDRESS(ES)

Seismological Laboratory 252-21
California Institute of Technology
Pasadena, CA 91125

AFOSR-TR-95 0493

ATION

9. SPONSORING / MONITORING AGENCY NAME(S) AND ADDRESS(ES)

Air Force Office of Scientific Research
110 Duncan Avenue, Suite B115
Bolling AFB
Washington DC 20332-0001
Attn: Code NM

nm

10. SPONSORING / MONITORING AGENCY REPORT NUMBER

11. SUPPLEMENTARY NOTES

12a. DISTRIBUTION / AVAILABILITY STATEMENT

Approved for public release; distribution unlimited

12b. DISTRIBUTION CODE

13. ABSTRACT *(Maximum 200 words)*

We present shock compression and release data for Coconino Sandstone, Solenhofen and Bedford limestones, and Chambless shale. Limestone, sandstones, and shale display three separate phases on the Hugoniot curve. For sandstone these are quartz, stishovite, and a dense liquid. The limestone Hugoniot phases are calcite I and a dense liquid, with an intervening phase of either calcite III or aragonite. For dense liquid SiO_2, ρ_0- 4.150 Mg/m^3 and K_{SO} = 313.5 GPa. For dense liquid $CaCO_3$, ρ_0 = 3.377 Mg/m^3 and K_{SO} = 139 GPa. Shock-induced phase transitions in both rocks are kinetically inhibited. Formulation of pressure phase can be modeled by $f = Ae^{-E_a/RT}$. For stishovite from quartz, A = 7.286 and E_a (kJ/mol) = 89.36-71.97 (ρ_0/ρ_{oo}), where ρ_o and ρ_{oo} are the non-porous and actual initial densities of the rock. $A = 6.245 \times 10^9$ and $E_a = 404+0.312\ \rho_{oo}$ for formation of SiO_2 liquid from stishovite. Carbonate-rich (~33% $CaCO_3$ by weight) shale has a bulk modulus of K_{SO} = 30.9 GPa. This appears to be the result of the clay/mica ratio and the presence of zeolitic water in the carbonate-rich shale rather than carbonate content. Carbonate-rich shale transforms to high-pressure phase assemblages, with marked increases in density (ρ = 3.6559, 3.740 Mg/m^3 for kaolinite, carbonate-rich and carbonate-poor shales, and slate, respectively, at P = 0), on shock compression. The behavior of this high pressure phase material is strongly influenced by the abundance of H_2O in the rock. Release adiabat data show conversion of high- to low-density material for shale upon release. Sandstone retains a factor of ~2 more shock energy than limestone, so decoupling of explosions from seismic waves will be more efficient in sandstones.

14. SUBJECT TERMS

15. NUMBER OF PAGES

16. PRICE CODE

17. SECURITY CLASSIFICATION OF REPORT	18. SECURITY CLASSIFICATION OF THIS PAGE	19. SECURITY CLASSIFICATION OF ABSTRACT	20. LIMITATION OF ABSTRACT
unclassified	unclassified	unclassified	SAR

Air Force Office of Scientific Research Contract No. F49620-92-J-0402 (CIT 64649)

SHOCK PROPAGATION IN CRUSTAL ROCKS: Sandstone, Limestone and Shale

July 1, 1992 to February 28, 1995

Thomas J. Ahrens
William W. Anderson
Yusheng Zhao

Seismological Laboratory
California Institute of Technology
Pasadena, CA 91125

April 1995

Final Report

Prepared for: Air Force Office of Scientific Research
110 Duncan Avenue, Suite B115
Bolling AFB
Washington, DC 20332-0001
Attn: Code NM

TABLE OF CONTENTS

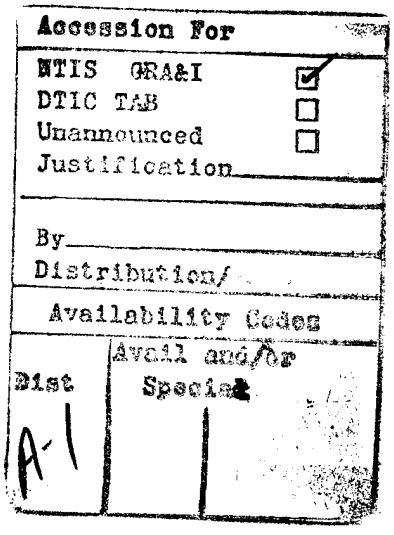

LIST OF ILLUSTRATIONS

LIST OF TABLES

SUMMARY

The shock Hugoniot and adiabatic release curves of sedimentary rocks display a range of different behaviors that affect the decay of shock waves propagating away form a confined source. Hysteresis in the shock-release paths of geologic materials results in irreversible energy deposition, thus depriving the shock wave of energy required to drive its propagation and resulting in a more rapid wave amplitude decay and less efficient coupling to far field seismic waves than would be expected from geometrical effects alone. Thus, data constraining this behavior in rocks are essential for determining the cavity volumes for various degrees of decoupling for different lithologies.

We have studied the shock compression and adiabatic release behavior of Coconino Sandstone with an initial density $\rho_{00} = 2.313$ Mg/m^3 and Solenhofen Limestone with initial density $\rho_{00} = 2.613$ Mg/m^3, a limestone from Bedford, Indiana, with initial density $\rho_{00} = 2.418$ Mg/m^3 and a calcareous shale from the Chambless formation with initial density $\rho_{00} = 2.576$ Mg/m^3. We used a series of shock Hugoniot and release adiabat measurements on sandstone, limestone, and shale to develop models for the shock and release behavior of these rocks. The sandstone shock Hugoniot curve can be calculated from the equations of state of quartz, stishovite, and a high coordination number liquid. A new fit of available data for the dense liquid phase gives $\rho_{00} = 4.150$ Mg/m^3, $K_{S0} = 313.5$ GPa, $K' = 1.8484$, $\gamma = 1.4(V/V_0)^{0.5}$, and $E_{tr} = 2.4$ MJ/kg. In the case of Coconino Sandstone, the presence of a few percent of non-quartz constituents requires that the STP densities of the relevant phases be reduced by 2.4% to fit the data. The mixed-phase regions of the Hugoniot can be modeled as a simple mixture of the two relevant end member phases. Formation of the higher pressure phase appears to be kinetically inhibited, with the fraction f of the higher pressure phase being described by $f = Ae^{-E_a/RT}$. For formation of stishovite from quartz, $A = 7.286$ and $E_a(\text{kJ / mol}) = 89.36 - 71.97(\rho_0/\rho_{00})$ where ρ_{00} and ρ_0 are the actual and theoretical nonporous densities of the initial rock sample. For formation of the dense liquid from stishovite, $A = 6.245 \times 10^9$ and E_a (kJ/mol) = $404 + 0.312\rho_{00}$. No formation of the higher pressure phase occurs until the phase boundary is reached. As crude approximations we describe the quartz-stishovite phase boundary by P = 12 GPa and the stishovite-dense liquid phase boundary by $T = 4348 - 12.121P$ for T in K and P in GPa.

Release adiabats from the single phase regions of the sandstone Hugoniot are modeled by the isentropes of the relevant phases. At ~5 GPa, stishovite begins to form a diaplectic glass. We model the release adiabat below this pressure as a straight line in P-V space, from the stishovite release isentrope at 5 GPa to the STP diaplectic glass density of 2.27 Mg/m^3. The dense liquid undergoes a similar change beginning at ~5 GPa with formation of normal silica glass with an STP density of 2.204 Mg/m^3. The quartz release adiabat follows the quartz isentrope to P=0. As with the Hugoniot, we model the release from the mixed-phase regions of the Hugoniot as a mixture of the relevant phases, with the proportions frozen at the Hugoniot values.

The limestone Hugoniot curve is complicated by several metastable phases and multiple-wave shock structure at low pressures. Single phase portions of the Hugoniots of Solenhofen and Bedford limestones are modeled as calcite I at low pressures and a dense liquid at high pressures. We have fit an equation of state for the dense liquid phase, with $\rho_0 = 3.377$ Mg/m^3, $K_{S0} = 139$ GPa, $K' = 3.4$, $\gamma = 2.5(V/V_0)$, and $E_{tr} = 2.142$ MJ/kg. At intermediate pressures, dense limestones such as Solenhofen seem to form calcite III, while the more porous Bedford limestone apparently forms aragonite. The mixed phase regions of the Hugoniot are modeled in a manner analogous to that used for the sandstone Hugoniot. The parameters describing the fraction f of the higher pressure phase in the mixed phase regions are $A = 5.848$ and $E_a = 62.713\text{-}20.651\rho_{00}$ for formation of calcite III or aragonite from calcite I and $A = 2.919$ and $E_a = 382.453\text{-}130.448\rho_{00}$ for formation of the dense liquid from either aragonite or calcite III, for E_a in kJ/mol and ρ_{00} in Mg/m^3. The phase boundaries in our model are approximated by $T_{I\text{-}Ar} = 164.7P\text{-}3.6$, $T_{I\text{-}III} = 78.00\text{-}1.3$, $T_{Ar\text{-}Liq} = 745+48P$, and $T_{III\text{-}Liq} = 401+25.8P$.

As with sandstone, we model the release adiabats with the isentropes of the relevant phases, mixing them at the appropriate ratios for release from the mixed-phase portions of the Hugoniot. There is no evidence of formation of a glass at very low pressures, but release of phases other than calcite I is apparently accompanied by decomposition with evolution of CO_2 gas at pressures below 1 GPa. We have ignored this very low pressure effect in our calculations.

Equation of state parameters for shale are calculated from the mineral composition, with the bulk modulus and its pressure derivative constrained by the shock wave data. The shale, which is composed of roughly equal amounts of quartz, calcite, and phyllosilicates, has a low pressure phase characterized by $\rho_0 = 2.615$ Mg/m^3, $K_{so} = 30.9$ GPa, $K' = 8.15$, and $\gamma = 0.73\ (v/v_0)^{1.52}$, and a high-

pressure phase with $\rho_0 = 3.659$ Mgkm^3, $K_{so} = 265$ GPa, $K' = 3.14$, and $\gamma = 1.2 (V/V_0)^{1.49}$. The release adiabats calculated from these equations of state generally agree with the data, but do not take into account large-volume phase changes that occur at low pressure.

These results allow us to estimate the fraction f' of shock internal energy irreversibly deposited in these rocks and thus no longer available to drive the shock wave. We find that f' is a factor of ~2 smaller in limestones than in sandstone, so that decoupling of the source from far-field seismic waves is more efficient in sandstones. The value of f' may be reduced considerably in the presence of an elastic precursor wave and of intermediate waves. Experimental evidence indicates that shock wave decay still occurs even in the supposedly purely elastic shock regime, suggesting that effects such as fracture formation are very important to the overall picture of explosive energy coupling.

I. INTRODUCTION

The shock Hugoniot and adiabatic release curves of sedimentary rocks display a range of different behaviors that affect the decay of shock waves propagating away form a confined source. Many of the minerals making up sandstones, shales, and limestones undergo phase transitions when shocked to pressures of interest to studies of coupling of energy from explosive sources into far field seismic waves. Both sandstones and limestones have been observed to exhibit elastic precursors and multiple wave behavior at shock velocities up to 3.7 km/s and 5.7 km/s, respectively [Ahrens and Gregson, 1964]. Hysteresis in the shock-release paths of materials results in irreversible energy deposition, thus depriving the shock wave of energy required to drive its propagation and resulting in a more rapid wave amplitude decay and less efficient coupling to far field seismic waves than would be expected from geometrical effects alone. Thus, data constraining this behavior in rocks are essential for determining the cavity volumes for various degrees of decoupling for different lithologies.

We have studied the shock compression and adiabatic release behavior of Coconino Sandstone with a mean initial density of $\rho_{00} = 2.313$ Mg/m^3 and Solenhofen Limestone with a mean initial density of $\rho_{00} = 2.613$ Mg/m^3, a limestone from Bedford, Indiana, with a mean initial density of $\rho_{00} = 2.418$ Mg/m^3, and a 2.62 Mg/m^3 calcareous shale (Chambless formation). The sandstone is primarily quartz, with ~3% feldspar. The limestones are essentially pure calcite with very minor amounts of other constituents. The shale is nearly equal fractions of calcite, clays and micas, and quartz.

II. SHOCK WAVE EQUATION OF STATE OF SANDSTONE, LIMESTONE, AND SHALE

A. Experimental Techniques.

The experimental techniques used for this study are discussed in detail elsewhere [Ahrens, 1987]. A sample of the rock being studied is placed on a metal driver plate (Figure 1), with standard buffers and/or inclined mirrors placed on the free (rear) surface of the sample. Shock arrival mirrors are placed against the rear surfaces of the driver plate, sample, and buffers. During the experiment, the driver plate is impacted by a gun-launched projectile containing a metal impactor (flyer plate). The impact generates a shock wave which propagates through the driver plate, sample, and buffer materials. Arrival of the shock wave at the free surface of each component of the target causes disruption of the specular reflection from the shock arrival mirrors as shown in Figure 1b. One spatial dimension of the target, including all shock arrival mirrors, is imaged as a function of time by a streak camera, allowing the shock wave transit times and thus the shock wave velocities through target components of known thickness to be determined. The internal energy E, pressure P, density ρ, and particle velocity u_p of the shocked sample and buffer are calculated from the measured projectile velocity, sample initial density, and shock wave velocity using the Rankine-Hugoniot shock equations for conservation of mass, momentum, and energy and by the requirement that pressure and particle velocity must be continuous across material interfaces.

The buffers and inclined mirrors are used to measure points on the release adiabats of the samples by the requirement that the P-u_p state in the released state of the sample be identical with that in the shocked buffer, or the free surface in the case of the inclined mirror. Table 1 give the properties of the materials used for flyer and driver plates and buffers in this study.

The shock Hugoniot of a material, which is the locus of final states achieved by shock compression, is conveniently described as a polynomial representation of the shock wave velocity, U_s in terms of the particle velocity, u_p:

$$U_s = C_0 + su_p + s' u_p^2 \qquad (1)$$

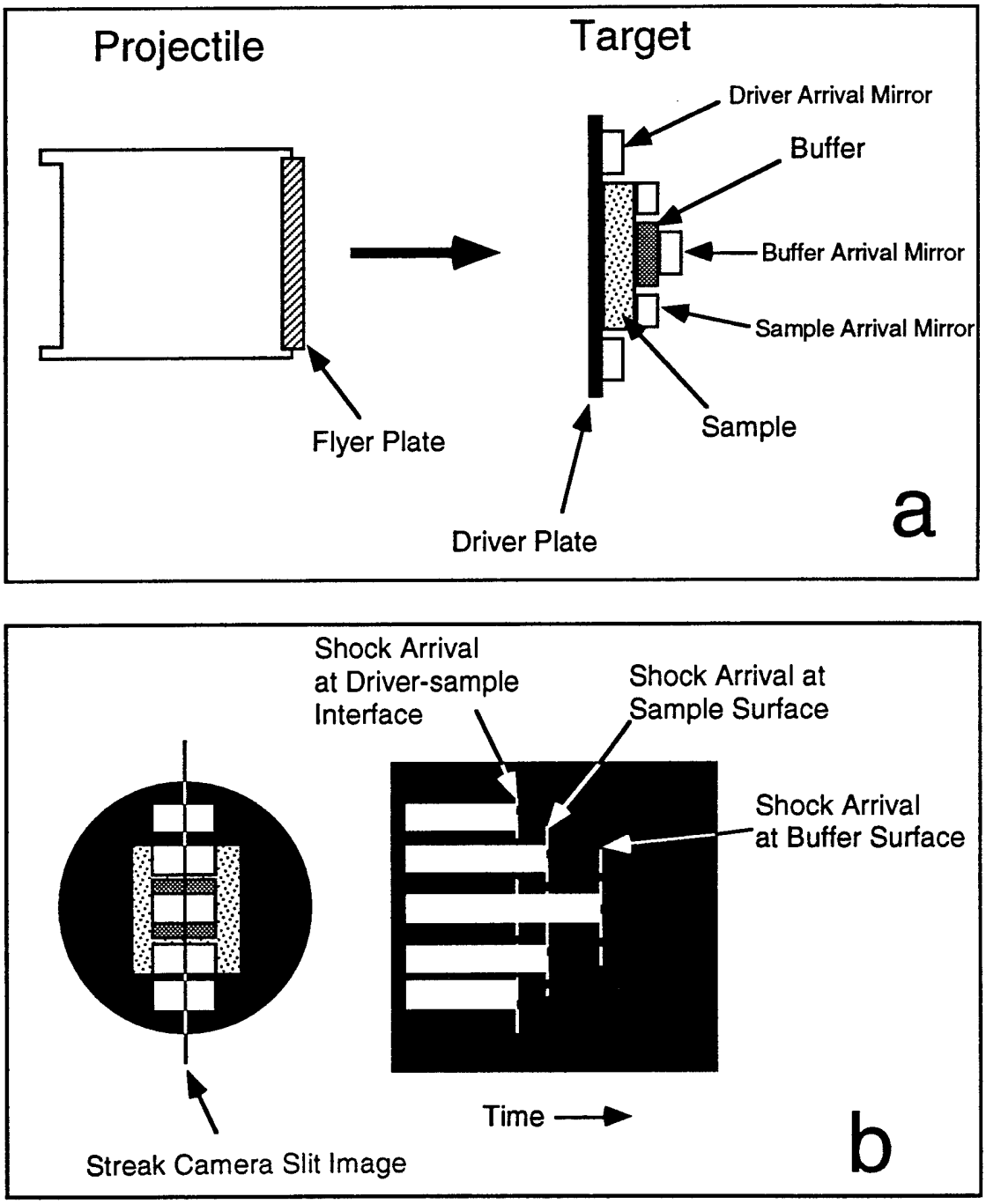

Figure 1. Diagram of a typical shock Hugoniot experiment with buffers for release adiabat measurements. (a) Projectile in flight prior to impact. (b) Static (left) and dynamic image recorded by streak camera.

Table 1. Shock Hugoniot parameters for standard materials used in this study.

Material	ρ_0 (Mg/m3)	C_0 (km/s)	s	s' (s/km)	Source
Al1100	2.707	5.386	1.339		1
Al2024	2.784	5.330	1.34		2
W	19.224	4.029	1.237		1
Ta	16.650	3.293	1.308		2
Lexan	1.193	2.449	1.498		3
		4.817	0.589		4
		1.907	1.431		5
Polystyrene	0.0474	0.362	0.9165	0.04982	6

(1) Marsh [1980]
(2) Mitchell and Nellis [1981]
(3) Fit to data from Marsh [1980] for $u_p \leq 2.605 \text{km/s}$.
(4) Fit to data from Marsh [1980] for $2.605 \text{km/s} < u_p \leq 3.456 \text{km/s}$.
(5) Fit to data from Marsh [1980] for $u_p \geq 3.456 \text{km/s}$.
(6) Calculated from ρ_{00} using expression from Anderson and Ahrens [1993]

Usually, the polynomial is truncated at first or second order. The pressure P, density ρ, and internal energy E in the shocked state are given by

$$P_H = \rho_{00} U_s u_p \tag{2}$$

$$\rho_H = \rho_{00} \frac{U_s}{U_s - u_p} \tag{3}$$

$$E_H = \frac{1}{2} u_p^{\,2} \tag{4}$$

Here, the subscripts 0 and H refer to the unshocked and shocked (Hugoniot) states, respectively, and the subscript 00 on ρ refers to the initial density, including any porosity in the sample. We arbitrarily set E = 0 as the initial condition.

B. Sandstone

1. Experimental Data

Table 2 presents the experimental data for the Coconino Sandstone used in this study, which had a mean initial bulk density of 2.313 Mg/m^3. The densities of the release states are upper limits, obtained by approximating the release paths as straight line segments in the P-V plane [Lyzenga and Ahrens, 1978].

Figure 2 shows the present data, along with an empirical fit to the U_s-u_p projection of the Hugoniot. The U_s-u_p projection of the Hugoniot curve can be divided into two straight-line segments with weighted fits of C_0 = 3.210±.026 km/s and s = 0.978±.011 for $u_p \leq$ 2.932 km/s and C_0 = 0.973±.108 km/s and s = 1.741±.036 for $u_p >$ 2.939 km/s. Also shown is the P-V projection of the curve described by the empirical U_s-u_p fit, along with the present data and data from Van Thiel [1977] for comparison.

Sandstones generally show an elastic precursor for very low shock pressures. Based on the data from Ahrens and Gregson [1964], the velocity U_{el} of the elastic precursor is only very weakly dependent on the particle velocity, with even the sign of the variation being uncertain. As a first order approximation, the elastic precursor velocity depends only on the initial density of the rock . Using the data from Ahrens and Gregson [1964], which cover polycrystalline quartz rocks

Table 2. Shock wave and release adiabat data for Coconino Sandstone.

Shot #	Initial Density (Mg/m^3)	Flyer/ Driver Material	Impact Velocity (km/s)	Shock State Particle Velocity (km/s)	Shock State Shock Velocity (km/s)	Shock State Pressure (GPa)	Shock State Density (Mg/m^3)	Release State Particle Velocity (km/s)	Release State Pressure (GPa)	Release State Density[a] (Mg/m^3)
913	2.3011 (0.0022)	Al2024	1.0259 (0.0027)	0.9210 (0.0027)	3.8893 (0.0315)	8.24 (0.07)	3.0150 (0.0091)	1.0698[b] (0.0605)	5.17 (0.39)	2.9509 (0.0755)
916	2.3623 (0.0026)	Al2024	1.5444 (0.0059)	0.9720 (0.0058)	4.2288 (0.0294)	9.71 (0.07)	3.0674 (0.0103)			
914	2.3299 (0.0023)	Al2024	1.9852 (0.0065)	1.2429 (0.0074)	4.5161 (0.0299)	13.08 (0.09)	3.2146 (0.0129)	1.5434[b] (0.0565)	8.77 (0.44)	3.0118 (0.1020)
911	2.3174 (0.0024)	W	1.7440 (0.0060)	1.5299 (0.0105)	4.8673 (0.0407)	17.26 (0.17)	3.3798 (0.0180)	1.9277[b] (0.0890)	12.27 (0.86)	3.0523 (0.2221)
908	2.3515 (0.0030)	W	2.3200 (0.0090)	2.0263 (0.0083)	5.1596 (0.0419)	24.59 (0.20)	3.8722 (0.0249)	2.3318[b] (0.0870)	16.53 (0.96)	3.7060 (0.1427)
261	2.3209 (0.0014)	Al1100/ Al2024	4.8409 (0.0060)	2.9261 (0.0106)	6.0658 (0.0116)	41.19 (0.16)	4.4838 (0.0184)	3.6503[c] (0.0351)	0.76 (0.02)	3.7060 (0.1427)
259	2.2847 (0.0014)	Ta	5.0697 (0.0043)	4.0803 (0.0072)	8.1038 (0.0615)	75.55 (0.49)	4.6017 (0.0409)	4.9849[b] (0.1160)	53.76 (2.24)	4.2374 (0.0348)
267	2.2793 (0.0041)	Ta	6.2287 (0.0083)	4.9353 (0.0247)	9.5250 (0.0941)	107.15 (1.03)	4.7303 (0.0624)	5.7989[b] (0.1403)	70.60 (3.10)	4.3139 (0.2103)
								7.6418[c] (0.3273)	3.72 (0.50)	3.5387 (0.2919)

(a) Using straight-line approximation of Lyzenga et al. [1983]
(b) Lexan buffer
(c) Polystyrene buffer

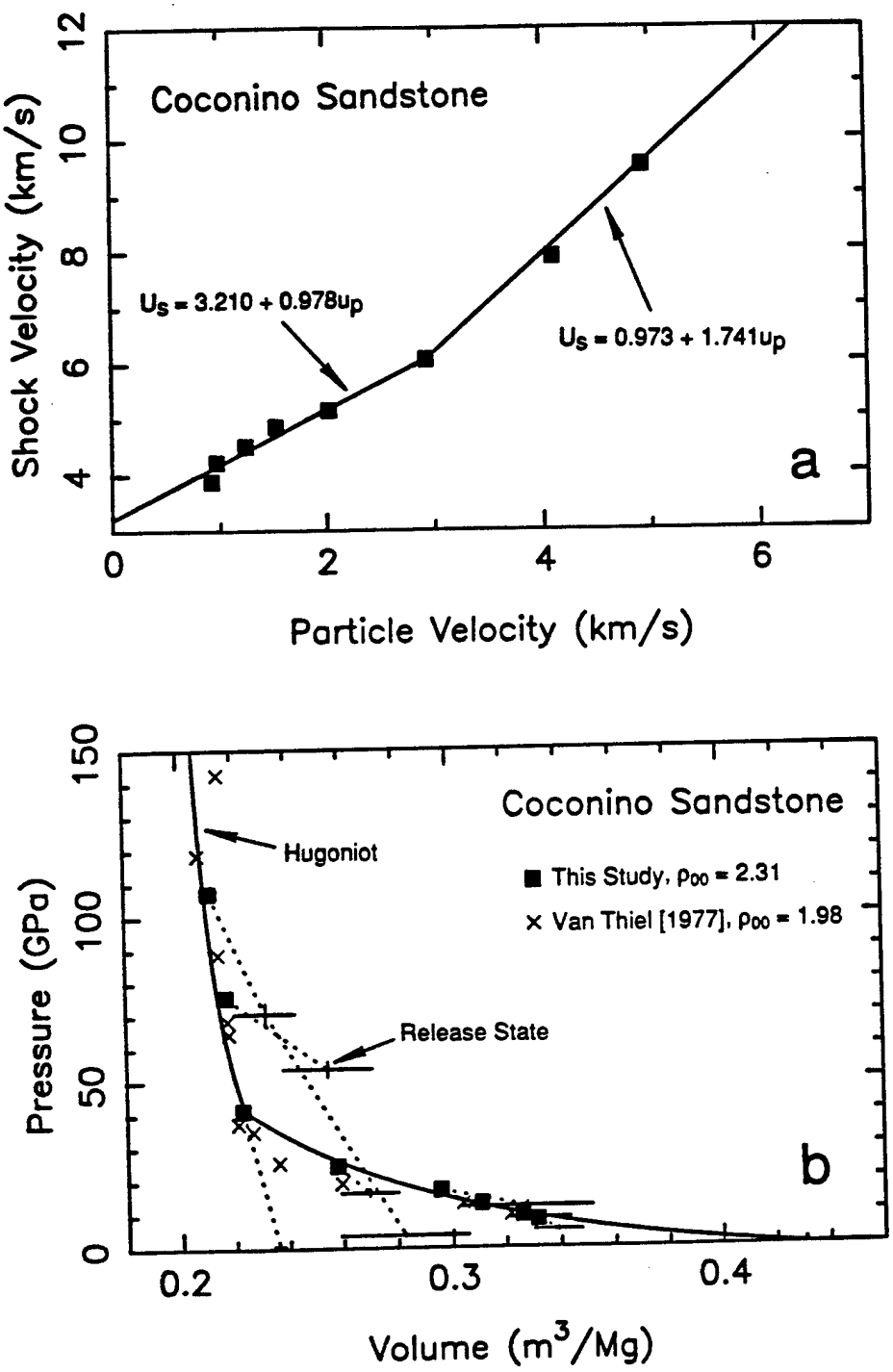

Figure 2. Shock Hugoniot and release adiabat data and Hugoniot based on empirical U_s-u_p fits for Coconino Sandstone. (a) U_s-u_p plane. (b) P-V plane.

with ρ_{00} in the range from 1.961 Mg/m^3 to 2.650 Mg/m^3, we describe the elastic precursor velocity U_{el} by

$$U_{el} = 4.53\rho_{00} - 6.122 \tag{5}$$

where U_{el} is given in km/s and ρ_{00} is in Mg/m^3.

2. Equation of State.

Although the experimental U_s-u_p relation gives us a good empirical description of the Hugoniot of the particular rock we studied, we wish to develop a model for shock and release behavior that is generally applicable to quartz rocks in general. Such a model could be easily modified to account for minor non-quartz constituents.

Since the predominant constituent is quartz, the phases appearing on the quartz shock Hugoniot curve are expected to also appear on the sandstone Hugoniot curve. In particular, these are quartz, stishovite, and dense SiO_2 liquid. Above the Hugoniot elastic limit (HEL), pressure at a given specific volume $V_H = 1/\rho_H$ on the Hugoniot can be calculated by

$$P_H = \frac{E_S + E_{tr} - P_S V_H/\gamma_H}{(V_{00} - V_H)/2 - V_H/\gamma_H} \tag{6}$$

where P_H is the shock state (Hugoniot) pressure, P_S is the pressure of the material on the principal isentrope at $V = V_H$, V_H is the shock state specific volume, V_{00} is the initial specific volume of the material, E_{tr} is the phase transition energy at STP, E_S is the internal energy gained in compression of the material along the principal isentrope to specific volume V_H, and γ_H = Grüneisen parameter of the material at volume V_H. This expression equates the energy at pressure P_H and specific volume V_H obtained by following the thermodynamic path of the shock compression (a straight line in P-V space) with that obtained via phase change (if needed) at room temperature and 1 bar pressure, isentropic compression to volume V_H, and isochoric heating to pressure P_H. We assume that the principal isentrope is described by the third order Eulerian finite strain Birch-Murnaghan equation:

$$P_S = \frac{3}{2}K_{S0}\left(x^7 - x^5\right)\left(1 + \xi - \xi x^2\right) \tag{7}$$

$$E_S = -\int_{V_0}^{V} P_S dV' = \frac{9}{2} V_0 K_{S0} \left[\frac{x^4}{4} - \frac{x^2}{2} + \frac{1}{4} - \xi \left(\frac{x^6}{6} - \frac{x^4}{4} + \frac{x^2}{2} - \frac{1}{6} \right) \right] \quad (8)$$

where

$$x = (V_0/V)^{1/3} \quad (9)$$

and

$$\xi = \frac{3}{4}(4 - K') \quad (10)$$

where K_{S0} is the value of the isentropic bulk modulus K_S at STP and K' in the isentropic pressure derivative of K_S at STP. We also assume that the Grüneisen parameter γ obeys

$$\gamma = \gamma_0 (V/V_0)^n \quad (11)$$

For the properties of quartz, we use the equation of state (EOS) parameters obtained by averaging the values given by Sumino and Anderson [1984]. For simplicity, we assume that C_V=3k/atom. For stishovite, we use the EOS parameters tabulated by Lyzenga et al. [1983], but with a slightly different value of K_{S0}, which seems to better describe the shock wave compression data for quartz given by Wackerle [1962] and presented graphically by Chhabildas [1986] and Lyzenga et al. [1983]. The shock temperature data of Lyzenga et al. [1983] suggest that SiO_2 is liquid above 117 GPa and 70 GPa on the quartz and fused quartz shock Hugoniots, respectively. Since our data are for samples which are only slightly more dense than fused quartz and the Coconino Sandstone data tabulated by Van Thiel [1977] are for densities lower than that of fused quartz, we can expect our highest pressure data to be for shock states in the liquid phase. The densities of the shock states for quartz and fused quartz in the relevant pressure ranges are incompatible with the known properties of liquid SiO_2 at low pressure and strongly suggest that the liquid phase on the Hugoniot is characterized by Si^{4+} in 6-fold coordination with O^{2-}, as it is in stishovite. This is a reasonable conclusion, since stishovite is the solid which would undergo equilibrium melting to give this liquid.

Lyzenga et al. [1983] give a set of EOS parameters for the dense liquid phase, but we cannot reconcile the resulting shock compression curves with all the existing Hugoniot data for quartz and fused quartz. We have refit the values of K_{S0} and K' to data from Lyzenga et al. [1983] for quartz, Trunin et al. [1971a] for porous quartz, Trunin et al. [1971b] for quartz and quartzite and, Lyzenga et al. [1983] and Marsh [1980] for fused quartz. We retain the empirical expression for C_V given by Lyzenga et al. [1983]. The resulting fit is shown in Figure 3. The EOS parameters used for the three phases of interest to this study are listed in Table 3, along with slight variations of these values which give a better fit to the data for Coconino Sandstone. The primary change made to bring the model in line with the data was to vary the values of ρ_0 for the different phases. This is presumed to reflect the effects of non-quartz constituents of the sandstone.

Above the HEL, the phase on the sandstone and quartz Hugoniots apparently remains quartz until sufficient energy is available to initiate transition to stishovite. Although part of the Hugoniot is in the coesite stability field, the available data show no evidence of coesite formation in the shock state. A wide mixed-phase (MP) region exists on the Hugoniot between the onset and completion of stishovite formation. The lower and upper pressure boundaries to this region depend on the value of ρ_{00}. The lower boundary on the MP regime occurs considerably above the pressure at which the Hugoniot enters the stishovite stability field, but decreases as ρ_{00} decreases, suggesting that the transition is kinetically inhibited (see, e.g., Podurets and Trunin [1987]). We can model the fraction f of the higher-pressure phase by assuming an Arrhenius rate constant for the transition and that the timescale for the transition is relatively constant (i.e., that the thickness of the shock front is proportional to U_s):

$$f = Ae^{-E_a/RT} \tag{12}$$

where the preexponential factor A and the activation energy E_a are determined empirically from the experimental data. The assumption here is that no transition occurs until the phase boundary is crossed, and then is controlled by (12) after the phase boundary is crossed. The issue of kinetics raises the possibility that specimen size could affect the behavior of the Hugoniot. However, this was experimentally tested by Podurets et al. [1976], who concluded that specimen size does not affect shock propagation or the position of the P-V Hugoniot curve. For the present model, we assume that the quartz-stishovite transition occurs at a set

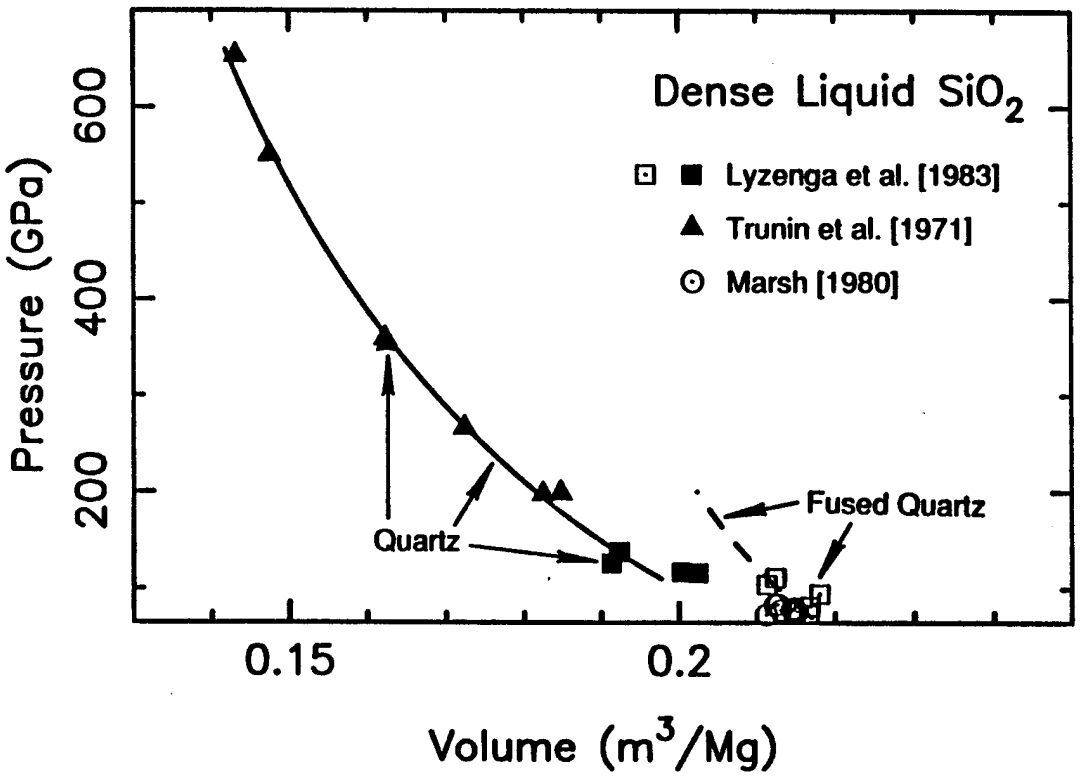

Figure 3. Equation of state fits to shock Hugoniot data for quartz and fused quartz in the high coordination number liquid stability region.

Table 3. Equation of state properties of phases for pure SiO_2 and Coconino Sandstone.

Property	Pure SiO_2			Coconino Sandstone		
	Quartz	Stishovite	Dense Liquid	"Quartz"	"Stishovite"	Dense Liquid
ρ_0 (Mg/m^3)	2650	4290.1	4150	2617	4187	4050
K_{S0} (GPa)	37.6	316	313.5	37.6	316	313.5
K'	6.31	5.4	1.8484	6.4	5.4	1.8484
γ_0	0.66	1.38	1.4	0.7	1.38	1.4
n	2.85	3.2	0.5	2.85	3.2	0.5
E_{tr} (MJ/kg)	0	0.82	2.4	0	0.82	2.4
C_V (J/kg/K)	1245.4	$736+.1102T^a$	$813+.1418T^a$	1245.4	$736+.1102T^a$	$813+.1418T^a$
Source	(1)	(2)	(3)	(1), (4)	(2), (4)	(3)

(a) Temperature in Kelvins.
(1) Sumino and Anderson [1984]
(2) Lyzenga et al. [1983], with K_{S0} modified for better fit to total data set
(3) This study, with C_V from Lyzenga et al. [1983]
(4) ρ_0 modified to better fit data

pressure of 12 GPa. To simplify the calculation from a practical standpoint, we also assume that the relevant temperature T is that for the lower pressure phase at the correct shock pressure. From the present data and data presented by Chhabildas [1986] for quartz and Van Thiel [1977] for Coconino Sandstone with $\rho_{00} = 1.98$ Mg/m^3, we find that the preexponential factor has a constant value of A = 7.286, while the activation energy obeys

$$E_a(kJ/mol) = 89.36 - 71.97(\rho_0/\rho_{00}) \tag{13}$$

where ρ_0 is the value for quartz.

The MP region is modeled by a volume weighted average of the Hugoniot curves of the low and high pressure phases in the P-V plane:

$$V_{MP} = fV_{HPP} + (1-f)V_{LPP} \tag{14}$$

where the subscripts LPP, MP, and HPP refer to the low pressure phase, mixed phase, and high pressure phase, respectively. This is not thermodynamically rigorous, but is convenient for the calculations and is a very good approximation, considering that thermal effects on V are fairly small at high pressures.

The transition region between stishovite and the high-density liquid can be treated in the same way as that between quartz and stishovite. The metastable Hugoniot curves in this region are very similar for the cases where data exist (i.e., on the quartz and fused quartz Hugoniot curves) so that the transition region is not readily apparent in the P-V data. However, the transition region is very apparent in the P-T data of Lyzenga et al. [1983]. We use a straight line fit to our interpreted phase boundary positions from Lyzenga et al. [1983] as the crudest representation of the stishovite-liquid phase boundary:

$$T = 4348 - 12.121P \tag{15}$$

for T in K and P in GPa. Their data show that, similar to the quartz-stishovite transition, the stishovite-liquid transition does not begin until the Hugoniot curve is well into the liquid stability region. The transition then occurs over a fairly narrow pressure range. The details of the transition region cannot be determined with confidence from the existing data, so we have chosen to express the fraction of liquid by (12), with $A = 6.245 \times 10^9$ and an activation energy given by

$$E_a(kJ/mol) = 404 + 0.312\rho_{00} \tag{16}$$

for ρ_{00} in kg/m^3.

Figure 4 shows the Hugoniot curves we calculate for quartz and Coconino sandstone using the EOS parameters in Table 3 and the kinetics model discussed above.

3. Release Adiabats.

The release adiabats of each of the Hugoniot phases can be calculated from the EOS parameters listed in Table 3, under the assumption that the constant volume specific heat, C_V, does not vary significantly, which is a reasonable approximation. For a given density ρ_r on the isentrope anchored to a shock state at density ρ_H and shock pressure P_H, the pressure P_r on the release isentrope is

$$P_r = P_{Sr} + (P_H - P_S)(V_H/V_r)^{n-1} \exp\left[\int_{V_r}^{V_H} (\gamma/V)dV\right] \tag{17}$$

where P_{Sr} is the pressure in the principal isentrope corresponding to $V = V_r$ in (7) - (9). The internal energy difference between this and the Hugoniot state (i.e., the energy converted from internal to kinetic energy by doing work to expand the material during the release process) is

$$E_H - E_r = E_H - E_{Sr} - \frac{V_r}{\gamma_r}(P_r - P_{Sr}) \tag{18}$$

where E_H is given by (4) The internal energy not converted into kinetic energy upon release is deposited as heat. This irreversible energy deposition causes the shock wave-release wave couple to decay as energy required to drive the wave propagation is sapped away.

The particle velocity of material released from the shocked state is related to the P-V release path via the Riemann integral formula [Rice et al., 1958]:

$$u_{pr} = u_{pH} + \int_{P_r}^{P_H} \left(-\frac{dV}{dP}\right)^{1/2}_{rel} dP \tag{19}$$

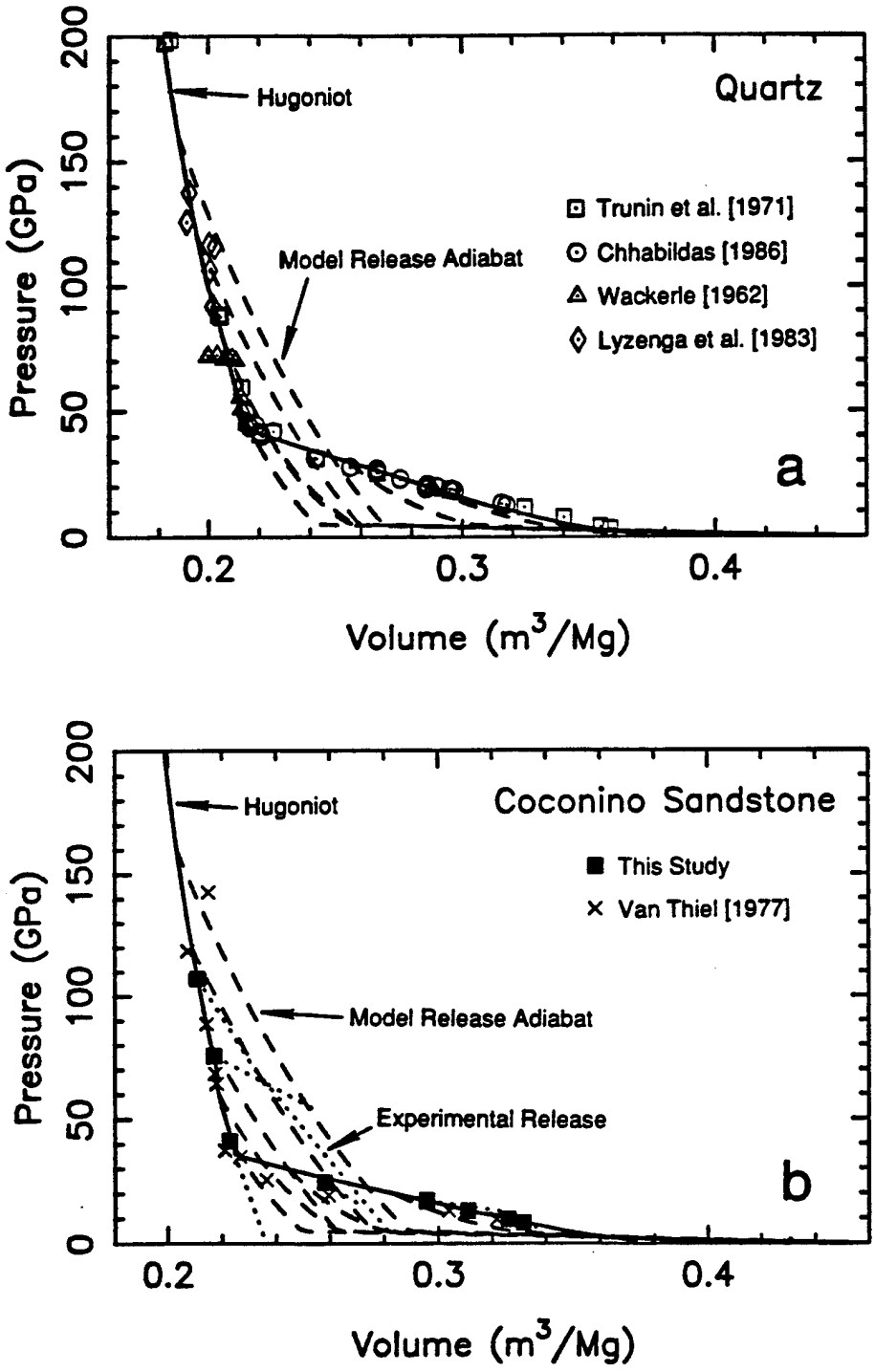

Figure 4. Model Hugoniots and release adiabats for (a) quartz and (b) Coconino Sandstone.

where the subscript rel refers to the isentropic release path. An additional contribution to u_{pr} can come from the energies of transition associated with phase changes during release. We have assumed that the total internal energy is constant with latent heat affecting sensible heat rather than macroscopic kinetic energy. The simplest model assumes that the relative fractions of the low and high pressure phases are kinetically frozen at their Hugoniot state values. The available evidence from recovered shocked quartz and from the present data is that the stishovite transforms to a diaplectic glass with an STP density of 2.27 Mg/m^3 and that dense amorphous SiO_2 transforms to the more familiar low-pressure glass (ρ = 2.204 Mg/m^3) or liquid at low pressures. Based on the available data, we assume this happens at a critical pressure P_c of ~5.1 GPa for both phases. In both cases, we have assumed that the path below P_c is a straight line in P-V space from the volume at P_c to the STP volume of fused quartz. This ignores the effects of thermal expansion, but the error introduced is insignificant. As with the Hugoniot, we model the release points on the mixed-phase release paths by assuming a mass-weighted average of the volumes of the low and high pressure phases via (14). Figure 4 presents release adiabats calculated with this model.

C. Limestone.

1. Experimental Data.

Table 4 presents the data obtained for Solenhofen and Bedford limestones in this study. Figures 5 and 6 present these data along with data from Ahrens and Gregson [1964], Van Thiel [1977], and Tyburczy and Ahrens [1986].

The low pressure behavior of $CaCO_3$ is very complicated. At least four phases are known which seem to be only slightly different in internal energy. In addition to calcite I and aragonite, at least two phases, calcite II and calcite III, are observed in static compression, with the calcite I-II and II-III transitions occurring at ~1.5 GPa and 2.2 GPa, respectively, at 298 K [Fiquet et al., in press]. Static compression data of Adadurov et al. [1960] also show a very slight volume discontinuity at ~1.16 GPa, although this could be due to some experimental effect. Complicating this issue is that, with the exception of calcite I, different investigators disagree markedly in their determinations of the properties of these phases.

Low pressure shock wave data for calcite and calcite rocks, including the data obtained in the present study, show not only an elastic precursor wave at low

Table 4. Shock wave and release adiabat data for Solenhofen and Bedford limestones.

Shot #	Rock	Initial Density (Mg/m^3)	Flyer/ Driver Material	Impact Velocity (km/s)	Shock State				Release State		
					Particle Velocity (km/s)	Shock Velocity (km/s)	Pressure (GPa)	Density (Mg/m^3)	Particle Velocity (km/s)	Pressure (GPa)	Density[a] (Mg/m^3)
925	Solenhofen	2.5928 (0.0027)	W	1.0000 (0.0034)	----[b]	5.6262[b,c] (0.1352)	----[b]	----[b]			
932	Solenhofen	2.6148 (0.0015)	W	1.5491 (0.0078)	----[b]	5.4734[b,c] (0.0312)	----[b]	----[b]			
931	Solenhofen	2.6195 (0.0035)	Al2024	1.0571 (0.0026)	0.1416[c] (0.0053)	5.1642[c] (0.0450)	2.08[c] (0.08)	2.7873[c] (0.0045)			
					0.3149[d] (0.0124)	4.3361[d] (0.0415)	4.04[d] (0.17)	2.8031[d] (0.0412)			
					0.6172 (0.0083)	4.0934 (0.0532)	7.24 (0.15)	3.0469 (0.0035)	2.0034[g] (0.1325)	0	1.6834 (0.1045)
926	Solenhofen	2.6150 (0.0024)	Al2024	1.9433 (0.0098)	1.1075[e] (0.0015)	5.1798[e] (0.0488)	15.00[e] (0.13)	3.3262[e] (0.0133)	1.6836[e,f] (0.0851)	9.98[e] (0.75)	2.7265[e] (0.2437)
922	Solenhofen	2.6193 (0.0018)	W	1.5300 (0.0088)	1.3029[e] (0.0076)	5.5346[e] (0.0358)	18.89[e] (0.15)	3.4258[e] (0.0101)			
921	Solenhofen	2.6189 (0.0033)	W	1.9993 (0.0072)	1.6826 (0.0062)	6.1574 (0.0283)	27.13 (0.15)	3.6037 (0.0097)	2.0242[f] (0.0886)	13.24 (0.88)	3.4978 (0.0712)
934	Bedford	2.4217 (0.0013)	Al2024	0.8394 (0.0044)	0.0686[c] (0.0035)	4.8119[c] (0.1664)	0.80[c] (0.05)	2.4567[c] (0.0880)			
					0.1163[d] (0.0050)	3.2789[d] (0.0795)	1.18[d] (0.07)	2.4938[d] (0.0880)			
					0.5677 (0.0073)	2.9121 (0.0655)	4.32 (0.11)	2.9739 (0.0013)	0.8535[g] (0.0580)	0	2.8156 (0.1003)
936	Bedford	2.4226 (0.0025)	Al2024	1.5427 (0.0072)	0.7472[c] (0.0105)	4.7672[c] (0.1238)	8.63[c] (0.26)	2.8729[c] (0.0160)			
					0.9372 (0.0113)	3.9975 (0.0413)	10.40 (0.20)	3.0512 (0.0025)	2.8108[g] (0.0576)	0	1.5033 (0.0378)

Table 4. (continued)

Shot #	Rock	Initial Density (Mg/m^3)	Flyer/ Driver Material	Impact Velocity (km/s)	Particle Velocity (km/s)	Shock Velocity (km/s)	Pressure (GPa)	Density (Mg/m^3)	Particle Velocity (km/s)	Pressure (GPa)	Density[a] (Mg/m^3)
935	Bedford	2.4148 (0.0026)	W	2.2770 (0.0085)	1.9471 (0.0077)	5.9542 (0.0413)	28.00 (0.20)	3.5882 (0.0156)	2.5891[f] (0.0467)	19.54 (0.50)	3.0539 (0.0974)
									5.9764[g] (0.0863)	0	1.0934 (0.0361)
264	Bedford	2.4220 (0.0017)	Al1100/ Al2024	5.0697 (0.0065)	2.8049 (0.0203)	7.5771 (0.1283)	51.48 (0.58)	3.8456 (0.0515)	3.8618[f] (0.1487)	34.25 (2.32)	3.0781 (0.2988)
									4.9112[h] (0.1309)	1.41 (0.13)	2.7901 (0.2630)
266	Bedford	2.4114 (0.0012)	Ta	6.0668 (0.0083)	4.6824 (0.0273)	10.4231 (0.2109)	117.71 (2.02)	4.3790 (0.0836)	6.0303[f] (0.4315)	75.80 (10.17)	3.6813 (0.6688)
									8.0372[h] (0.2934)	4.17 (0.50)	3.0500 (0.5239)

(a) Using straight-line approximation of Lyzenga et al. [1983]
(b) Due to experimental setup, only shock first wave velocity could be reliably determined.
(c) Elastic wave
(d) Intermediate wave
(e) Less reliable data
(f) Lexan buffer
(g) Free surface
(h) Polystyrene buffer

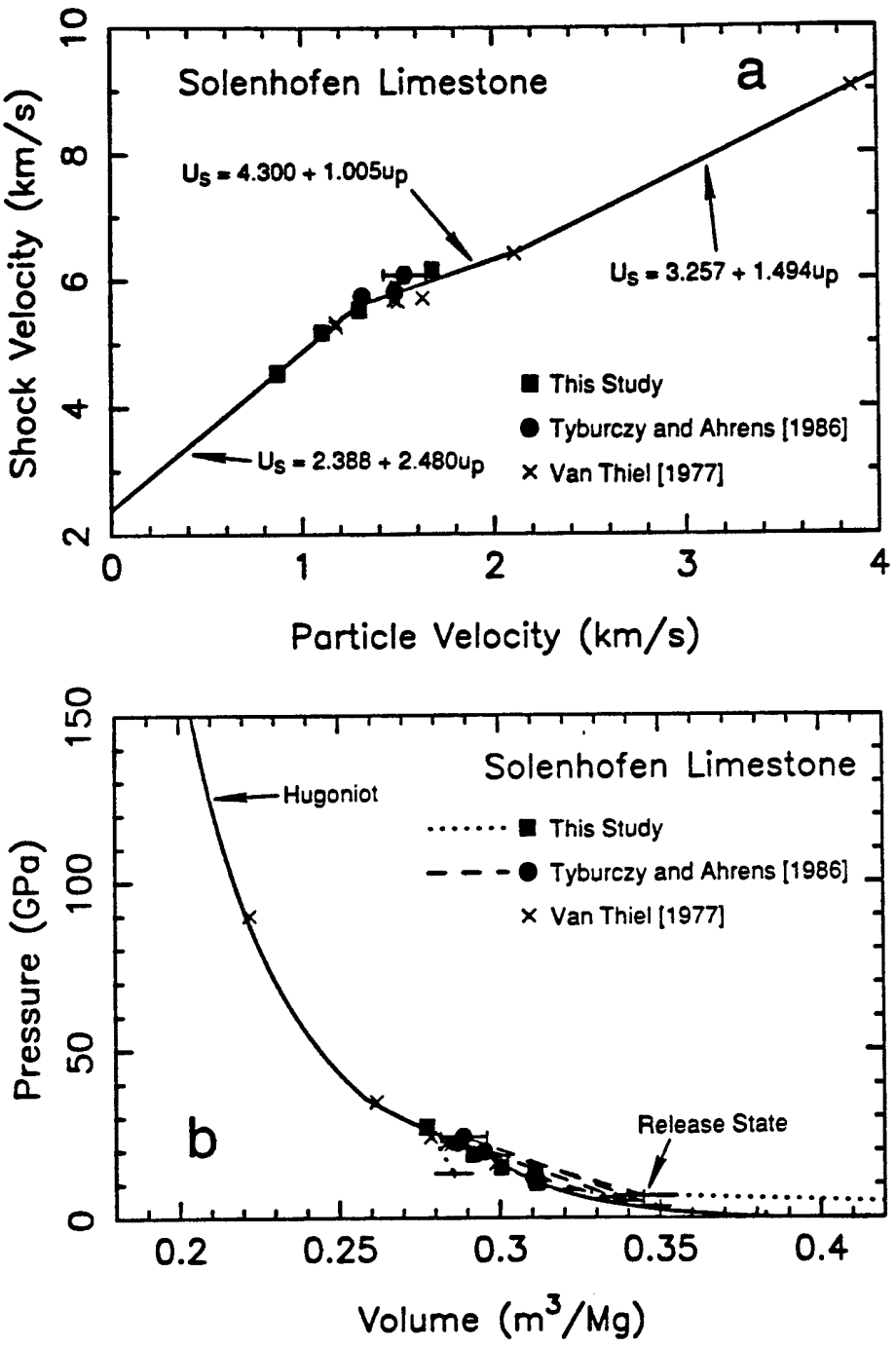

Figure 5. Shock Hugoniot and release adiabat data and Hugoniot based on empirical U_s-u_p fits for Solenhofen Limestone. (a) U_s-u_p plane. (b) P-V plane.

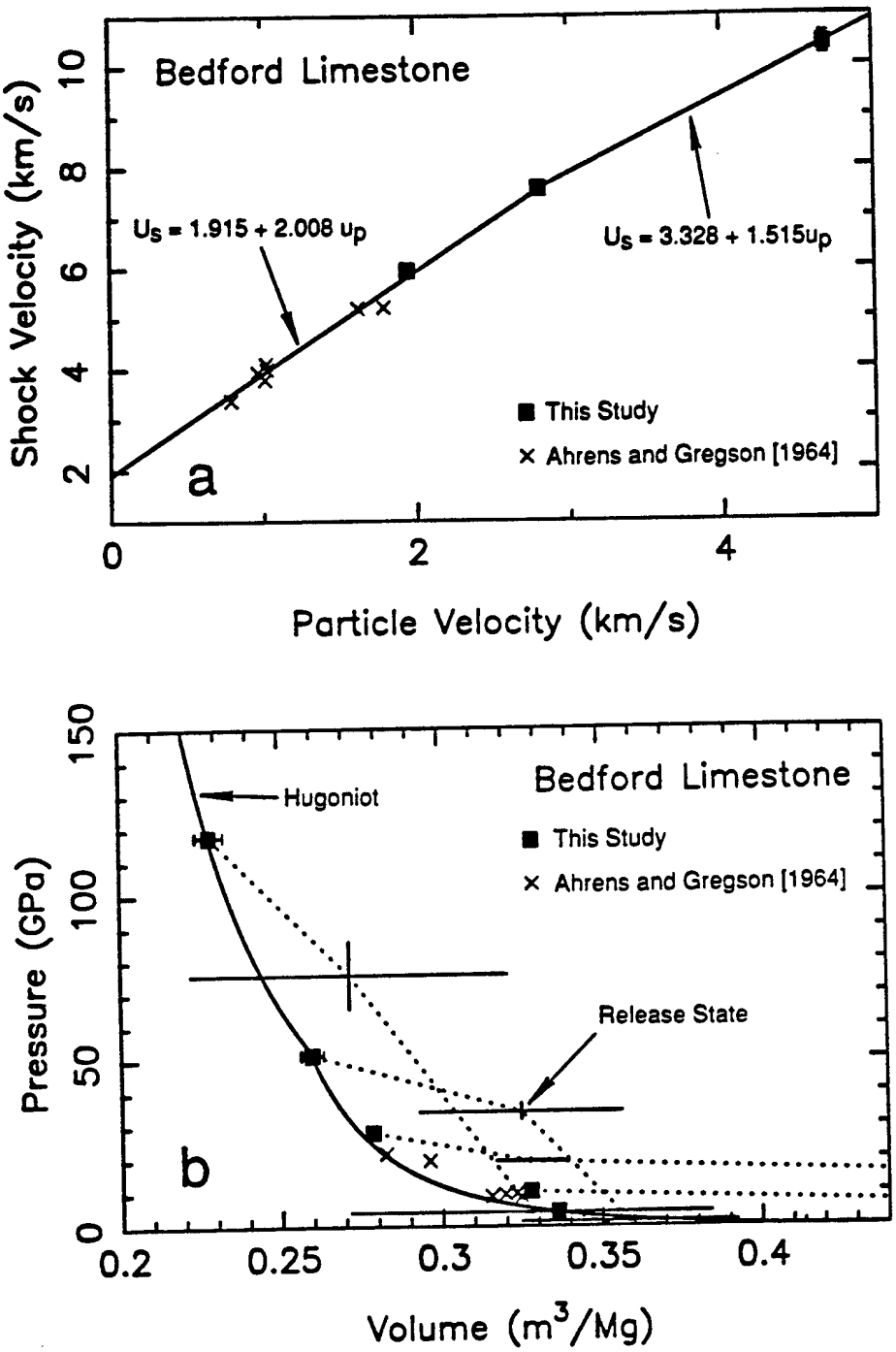

Figure 6. Shock Hugoniot and release adiabat data and Hugoniot based on empirical U_s-u_p fits for limestone from Bedford, Illinois. (a) U_s-u_p plane. (b) P-V plane.

shock stresses, but successive formation of at least two and perhaps three high-pressure phases, detected by the sequential arrival of multiple shock fronts. Although the data tend to be somewhat scattered, the stress levels of these different waves in the multiple-wave experiments are similar to those characterizing calcite II and III formation in static compression experiments.

As with sandstone, the velocity of the elastic precursor wave is not strongly correlated with particle velocity and is, to first order, a function only of the initial density of the limestone. We have combined the data of Ahrens and Gregson [1964] for the first wave velocities in polycrystalline calcite rocks with those from our experiments to obtain a data set for rocks with ρ_{00} in the range from 2.327 Mg/m^3 to 2.619 Mg/m^3. A fit of U_{el} as a function of ρ_{00} gives

$$U_{el} = -80.256 + 63.217\rho_{00} - 11.617\rho_{00}^{2} \qquad (20)$$

where U_{el} is in km/s and ρ_{00} is in Mg/m^3.

2. Equation of State.

Because of the confused nature of the $CaCO_3$ system at low pressures, we can provide only a very approximate treatment in that region. One very important complication is that the final shock states of calcite rocks below ~25 GPa cannot be matched by any published equation of state for any single phase of $CaCO_3$. We have chosen to model the lowest pressure portions of the Hugoniots of low-porosity calcite rocks as a mixture of calcite I and calcite III, where we identify calcite III as the phase observed by both Fiquet et al. [1993] and Vizgirda and Ahrens [1982]. In the case of Bedford limestone, (porosity ~ 12%), aragonite is used instead of calcite III, as explained below.

The identity of the phase comprising the final shock state just above this mixed phase region is uncertain. The shock compression data for single crystal calcite from Ahrens and Gregson [1964] seem to indicate that the final phase is not calcite III, but a higher pressure phase called calcite IV by Tyburczy and Ahrens [1986]. However, Fiquet et al. [1993] present new X-ray diffraction data which indicate that calcite III has the same properties as calcite IV given by Vizgirda and Ahrens [1982]. The previous EOS parameters for calcite III are called into question because the phase coexistence regions noted by Fiquet et al. [1993] can introduce errors into non-X-ray volume determinations used in the earlier studies. Fiquet et al. [1993] do note the appearance of new X-ray lines and a possible calcite IV phase

at about the same pressure as found by Ahrens and Gregson [1964], but the properties of this phase under shock compression seem to be consistent with calcite III, so the situation is at present confused. A further complication is that the Bedford Limestone Hugoniot above this point is more consistent with the properties of aragonite than calcite III. The issue will likely require further careful static X-ray diffraction experiments at elevated temperature and pressure to map out the phase diagram before it can be resolved.

Based on the available data and the EOS parameters presented by Fiquet et al. [1993] and Vizgirda and Ahrens [1982], we assume shock states in the 25-40 GPa range for calcite to be a single phase which we identify as calcite III. Based on the published data and previous determinations of EOS parameters, we propose that calcite III is described by ρ_{00} = 3.100 Mg/m^3, K_{S0} = 96.5 GPa, K' = 4.0, γ_0 = 1.183, n = 0.6, and E_{tr} = 0.02 MJ/kg. These parameters also describe the equivalent portions of the aragonite and relatively low porosity limestone Hugoniots reasonably well. For limestones with porosities as much as 15%, the corresponding region is better fit by aragonite.

Above the calcite III and aragonite single phase regions, the Hugoniot state appears to change to yet another phase. We fit the shock compression data for P > 100 GPa for calcite and limestones to obtain ρ_0 = 3.377 Mg/m^3, K_{S0} = 137 GPa, K' = 3.4, γ_0 = 2.5, n = 1.0, and E_{tr} = 2.142 MJ/kg. We presume that this phase probably is a dense melt, given the large STP transition energy from calcite I.

Table 5 summarizes the EOS parameters we have adopted for each phase considered in this study. We assumed in all cases that C_V = 3k/atom. Calcite II is not actually used in our study, but is presented for completeness. Another complication with calcite rocks is that no combination of the phases described in Table 5 will give the correct Hugoniots for highly porous rocks such as chalk (see, e.g., Kalashnikov et al. [1973], and Tyburczy and Ahrens [1986]). Because of the large internal energies induced by shock waves in porous materials, it is probable that the phases encountered on the Hugoniots of these materials are not the same as those found on the Hugoniots of the denser rocks studied here. We attempted to fit separate equations of state for the data for chalk, but still could not get consistent results. We suggest that the Hugoniot states of very porous calcite rocks may be affected by decomposition of the $CaCO_3$. Such behavior will exacerbate the difficulties of developing accurate models of the behavior of porous $CaCO_3$ rocks. At present, we advise that the models developed in this study be restricted to limestones with <20% porosity.

Table 5. Equation of state properties of $CaCO_3$ phases.

Property	Calcite I	Calcite II	Aragonite	Calcite III	Dense Liquid
ρ_0 (Mg/m^3)	2712	2522	2931	3100	3377
K_{s0} (GPa)	74.405	13	66.73	96.5	139
K'	5.42	4	4	4	3.4
γ_0	0.554	1.5	1.80	1.183	2.5
n	1	1	1	0.5	1
E_{tr} (MJ/kg)	0	0	-0.0006	0.02	2.142
C_v (J/kg/K)	1246	1246	1246	1246	1246
Source	(1)	(2)	(3)	(4)	(5)

(1) Sumino and Anderson [1984]
(2) Fit to data from Fiquet et al. [1993]
(3) Calculated from Salje and Viswanathan [1976] and Robie et al. [1978]
(4) Fiquet et al. [1993] and Vizgirda and Ahrens [1982]
(5) This study

As with the SiO_2 system, we model the mixed-phase regions of the Hugoniot by assuming kinetically-inhibited transformations on the equilibrium phase boundary is crossed. The primary reason for taking this assumption is the fact that formation of the high pressure phase identified as calcite III by Fiquet et al. [1993] above 2.2 GPa is not complete until ~25 GPa for single-crystal calcite under shock compression. Using the EOS parameters in Table 5 to calculate the Hugoniot temperatures corresponding to the P-V data, we fit Arrhenius parameters for (12) to get A = 5.848 and

$$E_a = 62.713 - 20.651\rho_{00} \tag{21}$$

for ρ_{00} in Mg/m^3 and E_a in kJ/mol for the conversion of calcite I to calcite III or aragonite. For the calcite III - liquid and aragonite - liquid mixed phase regions, we get A = 2.919 and

$$E_a = 382.453 - 130.448\rho_{00} \tag{22}$$

for ρ_{00} in Mg/m^3 and E_a in kJ/mol. For the calcite I-aragonite and calcite I-calcite III phase boundaries, we take the overall trends of the data presented by Jamieson [1957]:

$$T_{I-Ar} = 164.7P - 3.6 \tag{23}$$

$$T_{I-III} = 78.0P - 1.3 \tag{24}$$

for T in K and P in GPa. For the provisional calcite III-liquid and aragonite-liquid phase boundaries, we get

$$T_{Ar-Liq} = 745 + 48P \tag{25}$$

$$T_{III-Liq} = 401 + 25.8P \tag{26}$$

for T in K and P in GPa. These phase boundaries are extremely uncertain, being based solely on the behavior of the P-V Hugoniots and the temperatures calculated from the EOS parameters given in Table 5. Figure 7 presents the Hugoniots of Solenhofen and Bedford limestones calculated with this model.

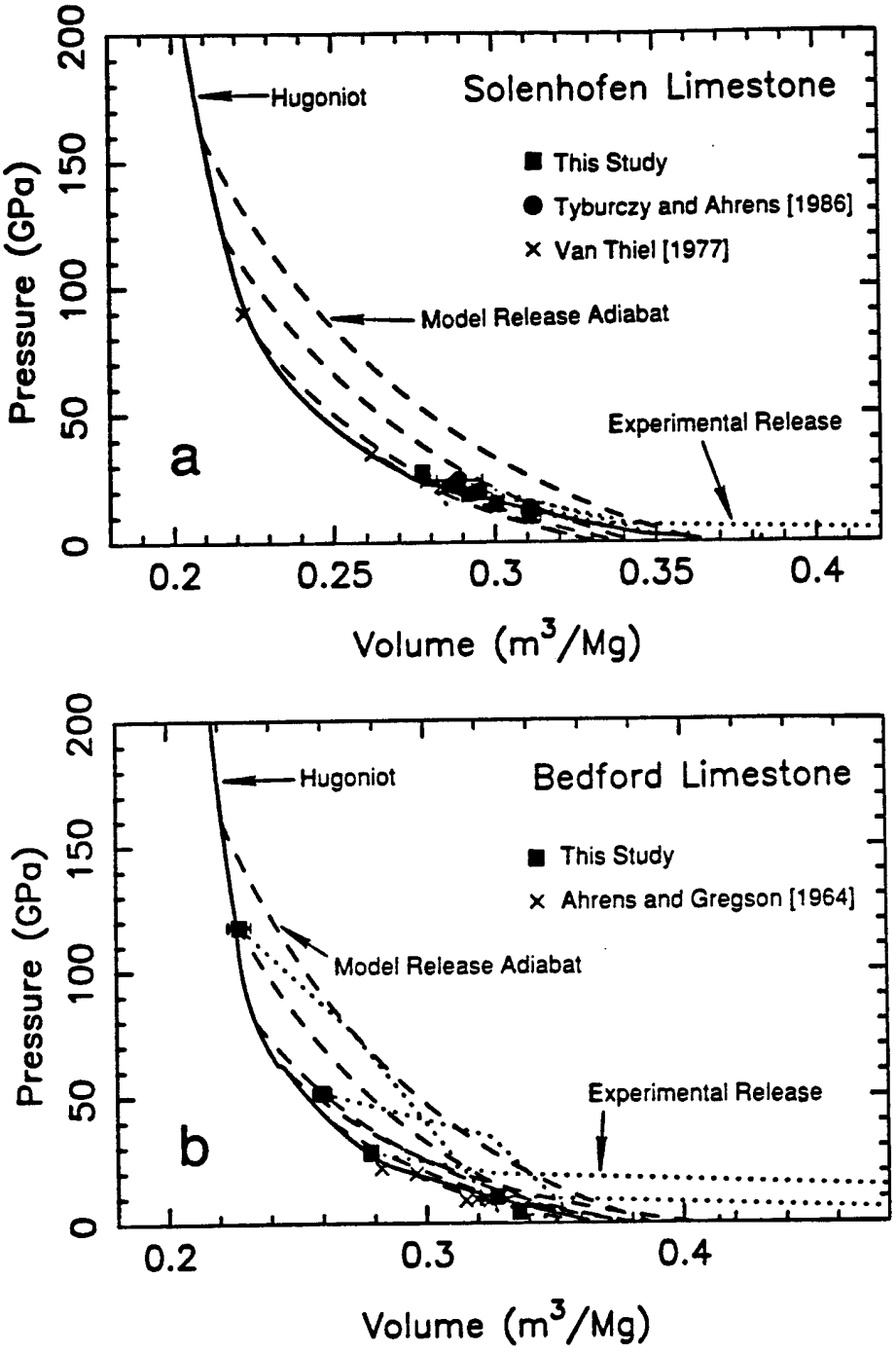

Figure 7. Model Hugoniots and release adiabats for (a) Solenhofen and (b) Bedford limestones.

3. Release behavior.

Measured points on release adiabats from the calcite III portion of the Hugoniot seem to require reversion to calcite I with energy approximately equal to the STP transition energy being converted to kinetic energy. One problem with this interpretation, however, is that the phase reversion takes place at a pressure higher than would be expected based solely on the $CaCO_3$ phase transition pressures. We may be detecting partial decomposition of calcite III or formation of a phase not yet identified. The final volumes of samples released from the calcite III region to P = 0 are large and suggest that CO_2 gas is being evolved at very low pressures. There is no evidence for this behavior at P = 1.41 GPa, so that the decomposition probably occurs at P < 1 GPa.

In contrast with release from calcite III, the liquid phase seems to be kinetically inhibited from freezing down to release state pressures as low as 4 GPa and follows the release isentropes described by (16). We suspect that this phase also undergoes decomposition with evolution of CO_2 at P < 1 GPa.

As with SiO_2, we model release from mixed-phase regions of the Hugoniot as release from the metastable Hugoniots of the two end-member phases at the same pressure. For this purpose, we assume that release from the calcite I metastable Hugoniot is the simple release isentrope described by (16). Release adiabats described by this model are shown in Figure 7.

D. Calcareous Shale

1. Samples.

A calcareous shale was collected, by us, for this study. It was obtained from the lower Chambless Limestone (Cambrian) in the southernmost Marble Mountains of the central Mojave Desert in California. Volatile-free oxide composition was determined via inductively-coupled plasma mass spectroscopy and X-ray fluorescence spectrometry. CO_2 in carbonates was determined by reaction with acid and volumetric measurement of gas evolved. The composition is given in Tables 6 and 7. The samples had a mean nonporous (crystal) density of 2.615 Mg/m^3 and a mean bulk density of 2.576 Mg/m^3. Ultrasonic measurements of longitudinal and transverse wave velocities give V_p = 4.505 km/s and V_s = 2.753 km/s, respectively.

Table 6.

Oxide composition analyses of Chambless calcareous shale from Marble Mountains, central Mojave Desert, California.

Oxide	Weight % (ICP)[a]	Weight % (XRF)[b]
SiO_2	44.59	44.20
TiO_2	0.84	0.76
Al_2O_3	9.68	9.42
Fe_2O_3	4.77	4.73
CaO	19.09	19.30
MgO	1.33	1.39
Na_2O	0.33	0.13
K_2O	2.04	2.25
CO_2[c]	14.34	14.34
H_2O[d]	4.21	3.46
Total	100.94	99.98

(a) Inductively-couple plasma source emission spectrometry

(b) X-ray fluorescence spectrometry

(c) Determined by gas evolution on treatment with acid.

(d) Determined by thermal desorption and decomposition (different samples).

Table 7

Mineral composition of calcareous shale used in this study, estimated from oxide composition and X-ray diffraction analysis.

Mineral	Weight Percent
Quartz	32.1
Calcite	32.6
Clays and Micas	34.4
Zeolitic Water	1.1
Total	100.2

2. Calcareous Shale, Experimental Results

Table 8 and Figure 8 present our results for calcareous shale. The U_s-u_p data can be broken down into three regions and fit by equation (1) truncated to first order. The fit parameters are C_0 = 3.803±0.097 km/s and s = 1.463±0.115 for u_p < 1.12 km/s, C_0 = 4.853±0.115 km/s and s = 0.523±0.073 for 1.12 ≤ u_p < 1.98 km/s, and C_0 = 2.405±0.139 km/s and s = 1.761±0.054 for u_p ≥ 1.98 km/s. The high compressibility shown at low pressures in the P-V data and the definitely defined segments of the U_s-u_p Hugoniot suggest that the lowest pressure data represent Hugoniot states entirely within the low-pressure phase of the shale and the highest pressure data represent states entirely within a high pressure phase. The intervening region represents a mixed-phase regime where the formation of the high pressure phase is incomplete, so that the Hugoniot states fall on a mixing line between the metastable extensions of the low and high pressure phase Hugoniot curves. We should note here that the term "phase" is not strictly correct, since the rock is a mixture of several different mineral phases. Rather, the term "low pressure phase" in the present context is used to refer to a material composed of the same mineral phases as the original sample, whereas the term "high pressure phase" refers to a material in which some or all of the constituent minerals have transformed to high pressure polymorphs. The term "mixed phase" in the present paper refers to a material in which minerals have partially transformed to high pressure polymorphs, but the transformation is incomplete.

In the lowest pressure experiments, the plastic shock wave in the shale was preceded by an elastic precursor. If we assume that the velocity U_{el} of elastic precursor should be identical to V_p under infinitesimal strain, then the elastic precursor obeys $U_{el} = 4.505 + 1.2u_p$ for U_{el} and u_p in km/s.

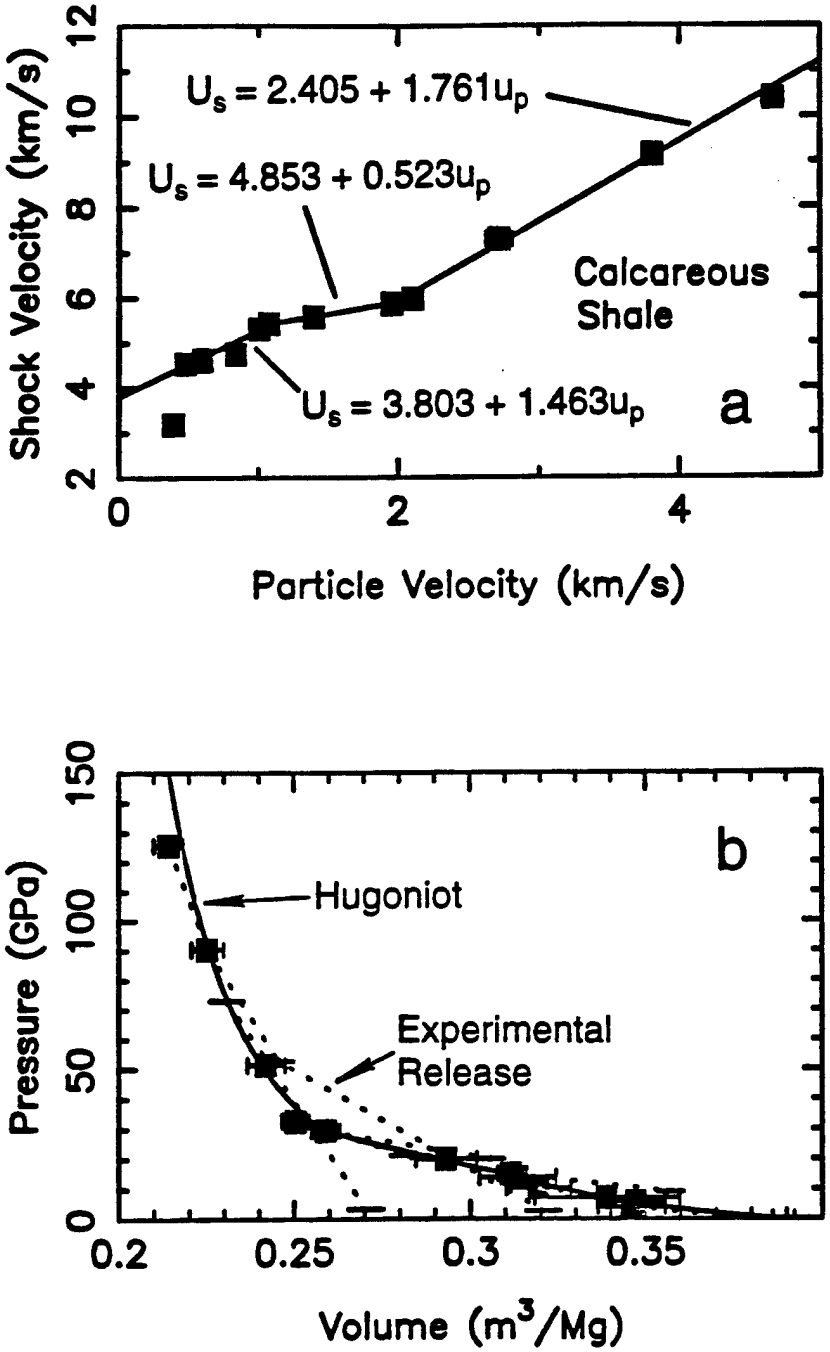

Figure 8. Experimental data for calcareous shale: (a) U_s-u_p projection with empirical fits to the data; (b) P-V projection of data and Hugoniot calculated from U_s-u_p fit.

Table 8
Experimental Data for Calcareous Shale.

Shot	Flyer/ Driver	Impact Velocity (km/s)	Sample Density (Mg/m^3)	Particle Velocity (km/s)	Shock Velocity (km/s)	Pressure (GPa)	Density (Mg/m^3)	Particle Velocity (km/s)	Pressure (GPa)	Density (Mg/m^3)
933	Al 2024	0.64 (0.01)	2.580	0.18[a] (0.02)	4.62[a] (0.09)	2.2[a] (0.2)	2.69[a] (0.07)			
				0.39[b] (0.03)	3.19[b] (0.04)	3.9[b] (0.2)	2.89[b] (0.08)	0.75 (0.07)	0 Free Surface	2.64 (0.06)
904	Al 2024	0.84 (0.02)	2.582	0.20[a] (0.02)	4.87[a] (0.09)	2.5[a] (0.2)	2.69[a] (0.07)			
				0.48[b] (0.02)	4.54[b] (0.05)	5.8[b] (0.2)	2.88[b] (0.07)	0.92 (0.05)	0 Free Surface	2.63 (0.05)
920	Al 2024	1.05 (.01)	2.566	0.60 (0.04)	4.62 (0.23)	7.1 (0.5)	2.95 (0.18)		VISAR	
912	Al 2024	1.44 (0.02)	2.574	0.84 (0.02)	4.76 (0.09)	10.3 (0.3)	3.13 (0.09)	1.17 (0.03)	5.9 (0.2) Lexan Buffer	2.90 (0.4)
								1.64 (0.09)	0 Free Surface	2.62 (0.06)
918	Al 2024	1.82 (0.01)	2.556	1.01 (0.04)	5.31 (0.15)	13.9 (0.5)	3.19 (0.11)		VISAR	
902	W	1.26 (0.02)	2.571	1.08 (0.02)	5.43 (0.05)	15.1 (0.4)	3.21 (0.04)	1.60 (0.02)	9.2 (0.3) Lexan Buffer	2.80 (0.03)
919	Al 2024	2.50 (0.01)	2.580	1.40 (0.04)	5.58 (0.12)	20.0 (0.6)	3.41 (0.10)		VISAR	

Table 8 (Continued)

Shot	Flyer/ Driver	Impact Velocity (km/s)	Sample Density (Mg/m^3)	Particle Velocity (km/s)	Shock Velocity (km/s)	Pressure (GPa)	Density (Mg/m^3)	Particle Velocity (km/s)	Pressure (GPa)	Density (Mg/m^3)
901	W	2.29 (0.02)	2.573	1.96 (0.03)	5.87 (0.06)	29.5 (0.5)	3.86 (0.06)	2.63 (0.03)	20.0 (0.3)	.327 (0.04)
								Lexan Buffer		
903	W	2.49 (0.02)	2.582	2.11 (0.04)	5.98 (0.09)	32.6 (0.8)	3.99 (0.06)	2.73 (0.01)	21.2 (0.9)	3.53 (0.07)
								Lexan Buffer		
263	Al 1100/ Al 2024	5.02 (0.02)	2.579	2.72 (0.09)	7.30 (0.08)	51.4 (2.1)	4.13 (0.09)	3.27 (0.08)	28.7 (0.9)	3.91 (0.07)
								Lexan Buffer		
								4.73 (0.09)	1.3 (0.1)	3.00 (0.05)
								Polystyrene Foam Buffer		
260	Ta	4.95 (0.02)	2.589	3.81 (0.05)	9.16 (0.12)	90.4 (0.9)	4.44 (0.09)	4.68 (0.02)	52.8 (0.9)	4.07 (0.07)
								Lexan Buffer		
								6.62 (0.03)	2.71 (0.19)	3.12 (0.05)
								Polystryene Foam Buffer		
265	Ta	6.13 (0.02)	2.582	4.67 (0.07)	10.40 (0.20)	125.6 (2.6)	4.67 (0.09)	5.62 (0.02)	73.0 (0.9)	4.33 (0.09)
								Lexan Buffer		
								7.28 (0.02)	3.34 (0.14)	3.70 (0.07)
								Polystyrene Foam Buffer		

[a]Elastic wave.
[b]Plastic wave.

3. Theoretical Equation of State of Shale.

The shale we studied is relatively carbonate rich (32.6% $CaCO_3$ by weight). The carbonate content of shales can be quite variable, so we have concentrated here on a carbonate-rich shale and use published data for carbonate-poor shales to obtain two different equations of state. We used the composition (Table 6), on an H_2O-free basis, to calculate the equivalent mineral mixture model of the rock, and then accounted for H_2O in the analysis and corundum in the norm by converting feldspars and other minerals to clays and micas. We represent H_2O bound in the structure of clays and micas as a separate constituent. Table 7 gives the resulting approximate mineral composition. The rock is composed of roughly equal amounts of quartz, clays, and calcite. This result is confirmed by powder X-ray diffraction analysis. The mean Archimedian value for ρ_0 of the low pressure phase is 2.615 Mg/m^3, with calculated values of $\gamma_0 = 0.73$, $n = 1.52$, $C_V = 1396$ Jkg^{-1}K^{-1}. We held K_{0S} at 30.9 GPa, calculated from (12), and find that the fit to the low pressure data not affected by an elastic precursor gives $K' = 8.15$. The calculated parameters for the high pressure phase are $\gamma_0 = 1.2$, $n = 1.49$, $E_{tr} = .42$ MJ/kg, and $C_V = 1396$ Jkg^{-1}K^{-1}. A fit to the four highest pressure shock compression data gives $\rho_0 =$ 3.659 Mg/m^3, $K_{0S} = 265$ GPa and $K' = 3.14$.

To study relatively carbonate-poor shales, we have combined the data of Trunin et al. [1988] and Al'tshuler and Pavlovskii [1971] for Russian shales and of Olinger [1978] for kerogen-free Chemung Shale. Trunin et al. [1988] give a chemical analysis of their shale, which we use as representative of all the samples, since the three data sets are the same within the scatter of the data. The analysis give ranges of abundances of different constituents, so that our estimation of the mineral content of the shales is only approximate. They also do not report an H_2O analysis but, based on the normative corundum abundance and the densities of the rocks, the dominant phyllosilicates are probably micas, rather than clays with the rock containing only ~8% $CaCO_3$. Table 9 gives the estimated mineral composition of these shales. We estimated ρ_0 for the low pressure phase on the assumption that all the normative corundum was in muscovite and get $\rho_0 = 2.813$ Mg/m^3. Other calculated parameters are $\gamma_0 = 0.79$, $n = 1.73$, and $C_V = 1159$ Jkg^{-1}K^{-1}. To avoid possible problems caused by elastic precursors in the original data, we fit the low pressure phase EOS to the data in the pressure range from 10 GPa to 16 GPa and get $K_{0S} = 61.1$ GPa and $K' = 4.52$. Calculated parameters for the high pressure phase are $\gamma_0 = 0.93$, $n = 1.92$, $C_V = 1159$ Jkg^{-1}K^{-1}, and $E_{tr} = 0.62$ MJ/kg. A fit to

data in the pressure range from 55 GPa to 120 GPa gives $\rho_0 = 3.740$ Mg/m^3, K_{0S}= 184 GPa and $K' = 3.24$.

Table 9

Estimated mineral composition of carbonate-poor shale studied by Trunin et al. [1988].

Mineral	Weight Percent
Quartz	40
Plagioclase	15
Pyroxene	13
Calcite	8
Muscovite	20
Magnetite	4
Total	100

4. Release Adiabats of Shale

Figure 9 presents the experimental *P-V* release adiabat points obtained in this study. In all cases, the release adiabats from the high pressure region of the Hugoniot parallel the *P-V* Hugoniot at high pressures, with deviation to larger volumes at lower pressures. Release from the mixed-phase regions seems generally to result in large volume increases probably related to reversion to the low pressure phase. Calcareous shale shows a large volume increase upon release, especially in the mixed-phase region, similar to the carbonate rocks and minerals [Vizgirda and Ahrens, 1982; Anderson and Ahrens, 1995]. The large volume increase at low pressures strongly suggest that the high pressure phase of shale reverts to the low pressure phase or to some other large-volume phase upon release.

As with the sandstone and limestone, the experimental release points can be used to check the validity of our equations of state. The points shown are actually lower limits on *V*, since the straight-line approximation of Lyzenga and Ahrens [1978] produces the lower extremum of thermodynamically allowable volume increase upon adiabatic release with no phase change. For a rigorous comparison, one would need to calculate the particle velocity increase for a test release path using the Riemann integral and compare that to the observed particle velocity increases. However, since the release state particle velocities often have fairly large uncertainties, the straight-line approximation of the release path is sufficient for the present study. We again make the assumption that C_V is constant so that eq. (17) can be used to calculate theoretical release adiabats. Figure 10 shows the release adiabats, calculated under the assumption that the high pressure phase is "frozen in" at the shock state mass fraction by kinetics. Reversion of the high pressure phase to some other lower density phase is manifested in the figures by experimental release paths at lower pressures that are shallower than the calculated paths. However, the higher pressure data generally show good agreement with the calculated release adiabats.

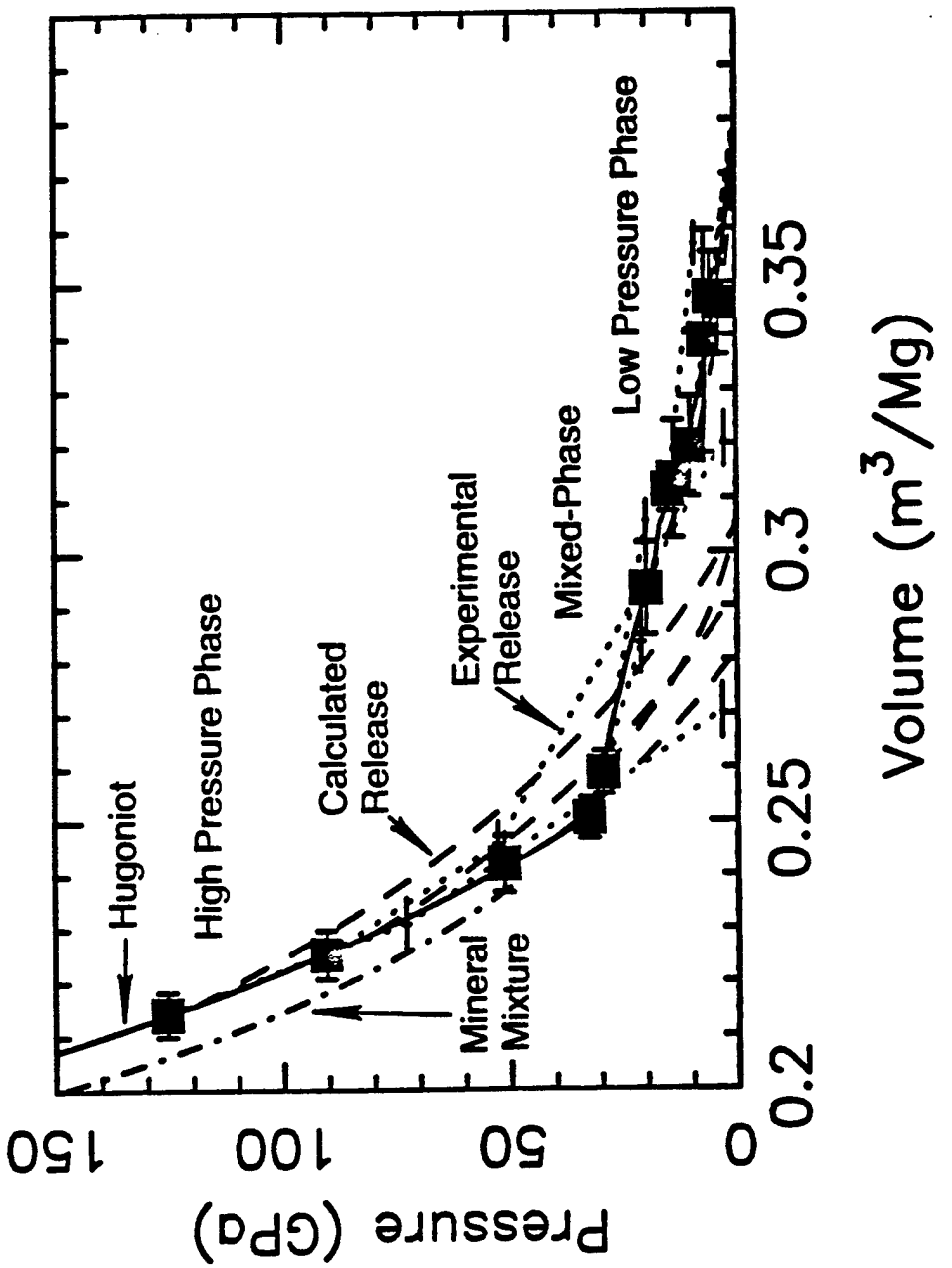

Figure 9. Calculated Hugoniot and release adiabats for calcareous shale, compared with the experimental data.

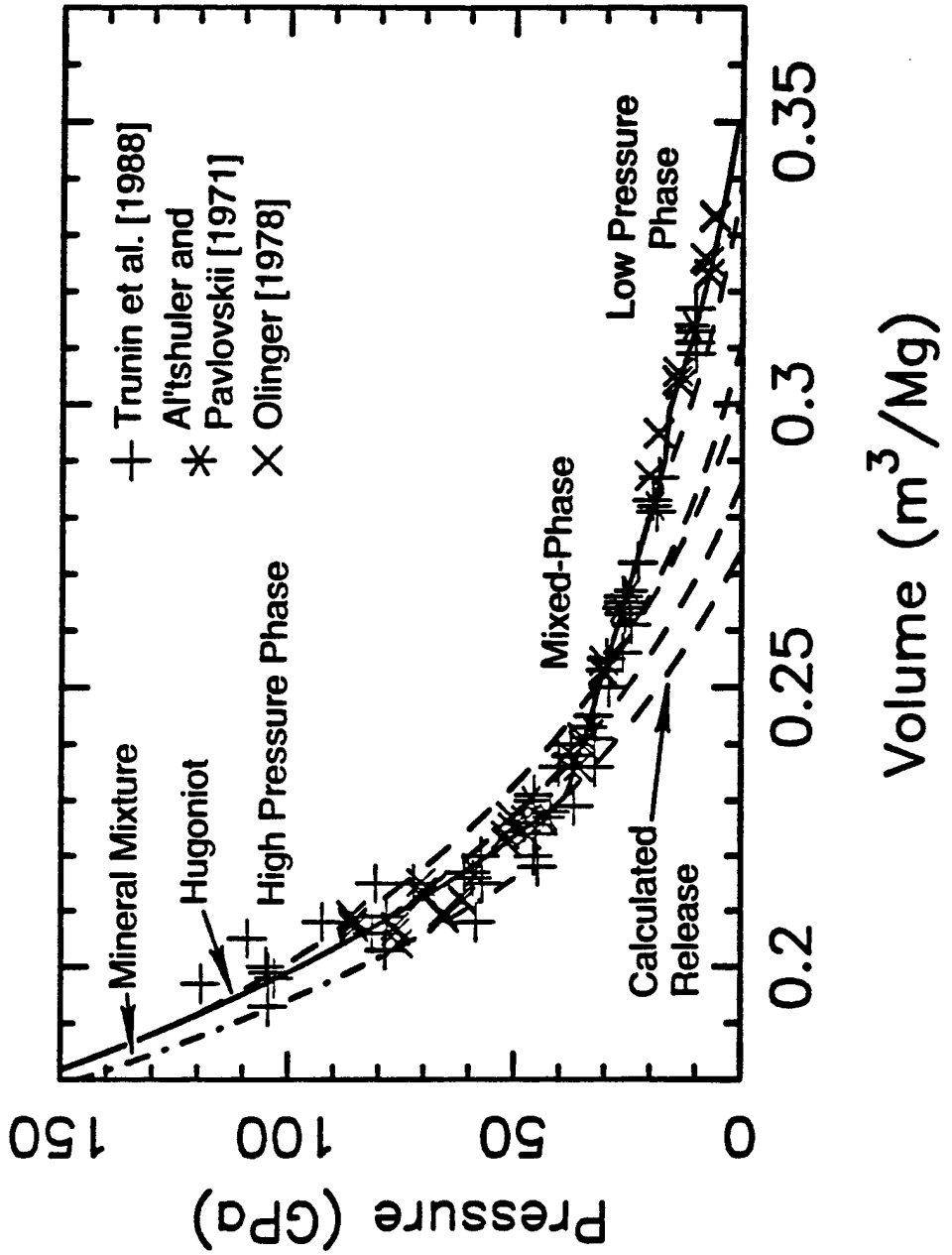

Figure 10. Calculated Hugoniot and release adiabats for carbonate-poor shale, compared with the experimental data.

III. DISCUSSION

Now that a model for the total shock-release cycle has been developed we can apply it to calculate the fraction f' of the shock internal energy E_H that is irreversibly deposited in the material for a given shock pressure using the equation

$$f' = \frac{E_H - E_r}{E_H} \tag{27}$$

where E_H and the quantity $(E_H - E_r)$ are given by (4) and (18), respectively. We have assumed here that the effects of the elastic precursor at low pressures can be ignored. The resulting estimates for f' are presented in Figures 11 and 12. For Coconino Sandstone, f' approaches 1 at low shock pressures because of pore collapse, but rapidly drops to ~0.44 at 18 GPa, rising rapidly to ~0.65 at 60 GPa and varying slowly thereafter, decreasing to ~0.59 at 200 GPa. In the case of the limestones, we have ignored the rapid expansion due to CO_2 gas evolution at extremely low pressures, so the values of f' given are upper limits in the case of release to P=0. At low pressures, as with sandstone, f' approaches 1 due to pore collapse, but drops rapidly, the rate of the drop being dependent on the initial density. Because of differences in the phases on the Hugoniot (aragonite in Bedford limestone versus calcite III in Solenhofen Limestone) and the difference in ρ_{00}, the P-f' curves behave very differently in detail below 120 GPa. Above 120 GPa, both curves are very similar, but with slightly greater energy deposition (higher f') in the more porous Bedford limestone, as should be expected.

There are some fundamental observations that should be made about the curves in Figure 11. The detailed structure of the curves should be taken with a fair amount of skepticism, since the models for the phase transition kinetics and the phase boundaries are based on sparse data. However, the relative positions of the curves is a property only of the equations of state thus should be a robust result. Since a higher value of f' is positively correlated with the irreversible energy deposition and thus the rate of decay of the shock wave, rocks characterized by high f' values will tend to decouple explosions from far field observables more efficiently than would rocks with low f' values. In particular, the conclusion from the curves presented in Figure 11 is that porous silicate rocks such as sandstones are much better suited to decoupling that are carbonate rocks. This is aside from other

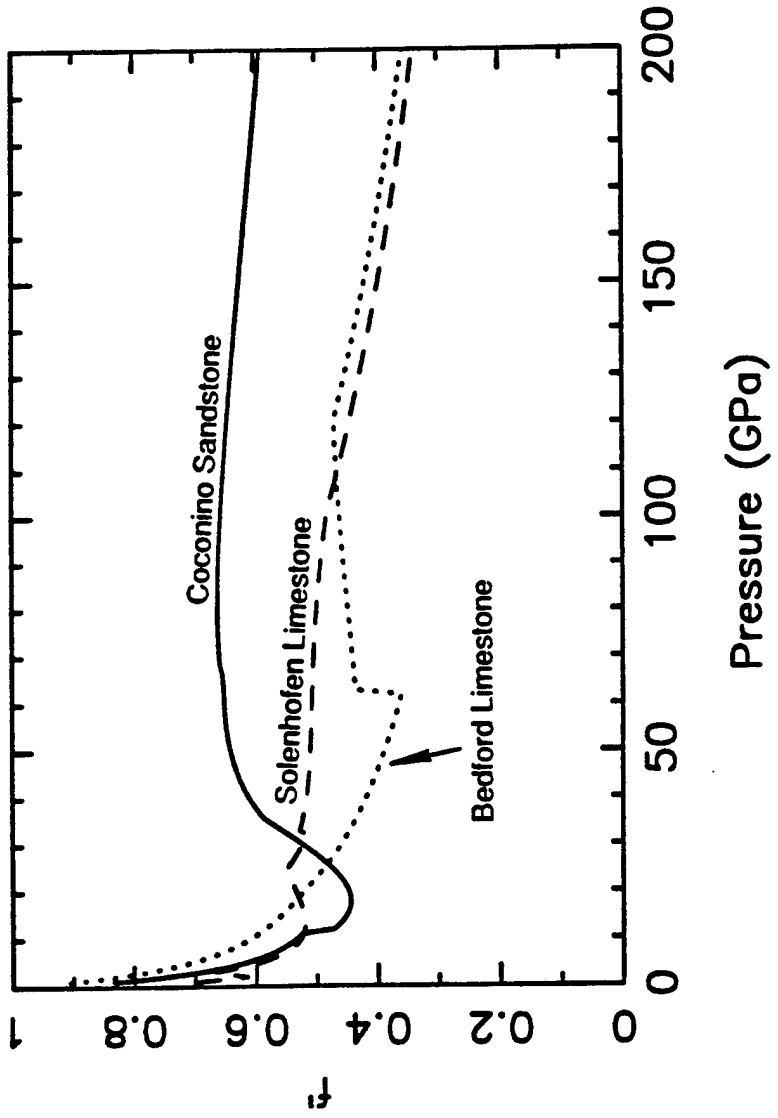

Figure 11. Fraction f' of Rankine-Hugoniot internal energy which is irreversibly deposited as heat in Coconino Sandstone and Solenhofen and Bedford limestones, shown as a function of peak shock pressure.

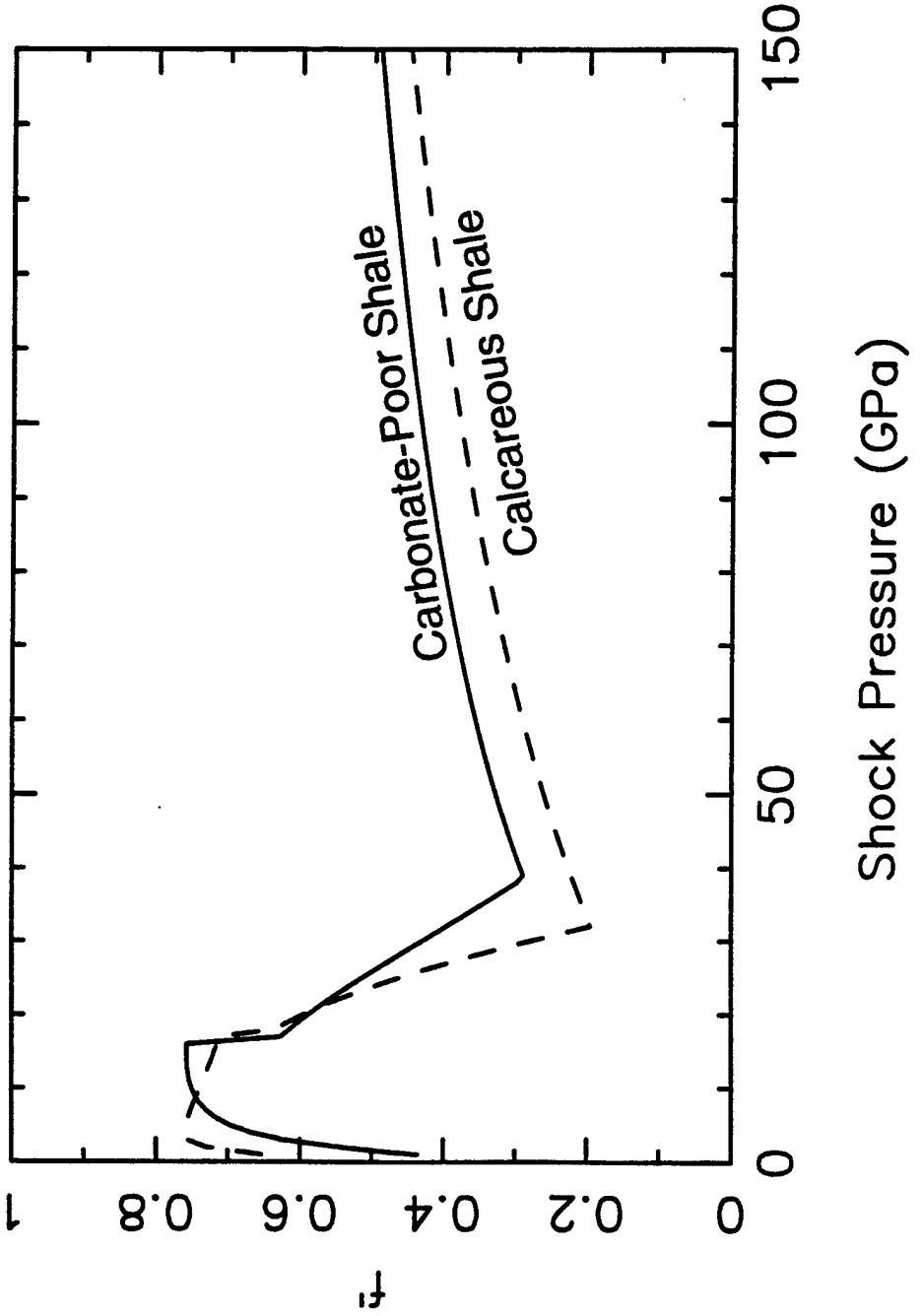

Figure 12. Fraction f' of Hugoniot internal energy irreversibly deposited in shale and slate, calculated assuming retention of the high pressure phase upon release. Actual energy deposition will be smaller.

issues, such as the need to contain gas evolved from decomposition of $CaCO_3$ as release pressures approach zero. Figure 12 summarizes the values of f' for the shales and slates.

An important effect which has been ignored here is the effect of the elastic precursor wave that precedes the plastic shock wave at low pressures. The actual values of E_H for our limestone experiments which showed elastic precursors and intermediate waves were ~35% and ~65% for Bedford and Solenhofen limestones, respectively, of the value that is calculated for the same final particle velocity in a purely plastic shock such as we have used in the present calculations. For the data from Ahrens and Gregson [1964] for Coconino Sandstone, the actual internal energy is ~55% of the calculated plastic shock energy. Also, material strength in mitigating pore collapse at low pressures, so that the energy deposition is much lower. Since the release behavior should be the same, however, the result is that at very low pressures, even in porous materials, f'~0. There is ample experimental evidence that significant energy deposition is occurring at low shock pressures, however, so that processes such as fracture formation must be important to the overall question of coupling of the near-source behavior to far-field observables.

IV. CONCLUSIONS

We have performed a series of shock Hugoniot and release adiabat measurements on sandstone, limestone, and shale and combined the results with previous data to develop models for the shock and release behavior of these rocks. The single-phase portions of the sandstone Hugoniot curve can be calculated from the equations of state of quartz, stishovite, and a high coordination number liquid. The properties of quartz and stishovite have been extensively studied in the past. We present a new fit of available data for the dense liquid phase to get $\rho_{00} = 4.150$ Mg/m^3, $K_{S0} = 313.5$ GPa, $K' = 1.8484$, $\gamma = 1.4(V/V_0)^{1/2}$, and $E_{tr} = 2.4$ MJ/kg. In the case of Coconino Sandstone, the presence of a few percent of non-quartz constituents requires that the STP densities of the relevant phases be reduced by 2.4% to fit the data. The intervening mixed-phases region can be modeled as a simple mixture of these two relevant end member phases under the assumption that formation of the higher pressure phase is kinetically inhibited. The fraction f of the higher pressure phase is described by $f = Ae^{-E_a/RT}$. For formation of stishovite from quartz, $A = 7.286$ and $E_a(\text{kJ / mol}) = 89.36 - 71.97(\rho_0/\rho_{00})$ where ρ_{00} and ρ_0 are the actual and theoretical nonporous densities of the initial rock sample. For formation of the dense liquid from stishovite, $A = 6.245 \times 10^9$ and E_a (kJ/mol) = $404 + 0.312\rho_{00}$. No formation of the higher pressure phase occurs until the phase boundary is reached. As crude approximations we describe the quartz-stishovite phase boundary by P = 12 GPa and the stishovite-dense liquid phase boundary by $T = 4348 - 12.121P$ for T in K and P in GPa.

Release adiabats from the single phase regions of the sandstone Hugoniot are modeled by the isentropes of the relevant phases, as described by the equation of state. At ~5 GPa, stishovite begins to form a diaplectic glass. We model the release adiabat below this pressure as a straight line in P-V space, from the stishovite release isentrope at 5 GPa to the STP diaplectic glass density of 2.27 Mg/m^3. The dense liquid undergoes a similar change beginning at ~5 GPa with formation of normal silica glass with an STP density of 2.204 Mg/m^3. The quartz release adiabat follows the quartz isentrope to P=0. As with the Hugoniot, we model the release from the mixed-phase regions of the Hugoniot as a mixture of the relevant phases, with the proportions frozen at the Hugoniot values.

The limestone Hugoniot curve is complicated by several metastable phases and multiple-wave shock structure at low pressures. Single phase portions of the Hugoniots of Solenhofen and Bedford limestones are modeled as calcite I at low

pressures and a dense liquid at high pressures. We have developed an equation of state for the dense liquid phase, with ρ_0 = 3.377 Mg/m^3, K_{S0} = 139 GPa, K' = 3.4, $\gamma = 2.5(V/V_0)$, and E_{tr} = 2.142 MJ/kg. At intermediate pressures, dense limestones such as Solenhofen seem to form calcite III, while the more porous Bedford limestone apparently forms aragonite. The mixed phase regions of the Hugoniot are modeled in a manner analogous to that used for the sandstone Hugoniot. The parameters describing the fraction f of the higher pressure phase in the mixed phase regions are A = 5.848 and $E_a = 62.713\text{-}20.651\rho_{00}$ for formation of calcite III or aragonite from calcite I and A = 2.919 and $E_a = 382.453\text{-}130.448\rho_{00}$ for formation of the dense liquid from either aragonite or calcite III, for E_a in kJ/mol and ρ_{00} in Mg/m^3. The phase boundaries in our model are approximated by $T_{I\text{-}Ar} = 164.7P\text{-}3.6$, $T_{I\text{-}III} = 78.00\text{-}1.3$, $T_{Ar\text{-}Liq} = 745+48P$, and $T_{III\text{-}Liq} = 401+25.8P$.

As with sandstone, we model the release adiabats with the isentropes of the relevant phases, mixing them at the appropriate ratios for release from the mixed-phase portions of the Hugoniot. There is no evidence of formation of a glass at very low pressures, but release of phases other than calcite I is apparently accompanied by decomposition with evolution of CO_2 gas at pressures below 1 GPa. We have ignored this very low pressure effect in our calculations.

Equation of state parameters for shale are calculated from the mineral composition, with the bulk modulus and its pressure derivative constrained by the shock wave data. The shale, which is composed of roughly equal amounts of quartz, calcite, and phyllosilicates, has a low pressure phase characterized by ρ_0 = 2.615 Mg/m^3, K_{so} = 30.9 GPa, K´ = 8.15, and $\gamma = 0.73\ (v/v_0)^{1.52}$, and a high-pressure phase with ρ_0 = 3.659 Mgkm^3, K_{so} = 265 GPa, K´ = 3.14, and $\gamma = 1.2\ (V/V_0)^{1.49}$. The release adiabats calculated from these equations of state generally agree with the data, but do not take into account large-volume phase changes that occur at low pressure.

Use of these results allows us to estimate the fraction f' of shock internal energy irreversibly deposited in these rocks. This energy in no longer available to drive the shock wave, so the shock wave decays more rapidly than expected from geometric effects alone. We find that f' is a factor of ~2 smaller in limestones than in sandstone, so that decoupling of the source from far-field seismic waves is more efficient in sandstones. This analysis ignored the effects of material strength at low shock pressures, although such effects are important. The value of f' may be reduced considerably in the presence of an elastic precursor wave and of intermediate waves. Experimental evidence indicates that shock wave decay still

occurs even in the supposedly purely elastic shock regime, showing that effects such as fracture formation are very important to the overall picture of explosive energy coupling.

V. REFERENCES

Adadurov, G. A., D. B. Balashov, and A. N. Dremin, A study of the volumetric compressibility of marble at high pressures, Izv. Earth Phys. (Engl. Trans.), 463-466, 1960.

Ahrens, T. J., Shock wave techniques in geophysics and planetary physics, in Methods of Experimental Physics, 24, (C. G. Sammis and T. L. Henyey, eds.), Academic Press, San Diego, pp. 185-235, 1987.

Ahrens, T. J., and V. G. Gregson, Shock compression of crustal rocks: data for quartz, calcite, and plagioclase rocks, J. Geophys. Res., 69, 4839-4874, 1964.

Anderson, W. W., and T. J. Ahrens, Physics of interplanetary dust capture via impact into organic polymer foams, J. Geophys. Res., in press, 1993.

Chhabildas, L. C., Shock loading and release behavior of x-cut quartz, in Shock Waves in Condensed Matter (Y. M. Gupta, ed.), New York, Plenum, 601-605, 1986.

Fiquet, G., F. Guyot, and J.-P. Itié, High-pressure X-ray diffraction study of carbonates: $MgCO_3$, $CaMg(CO_3)_2$, and $CaCO_3$, Am. Mineral., in press, 1993.

Jamieson, J. C., Introductory studies of high-pressure polymorphism to 24,000 bars by X-ray diffraction with some comments on calcite II, J. Geology, 65, 334-343, 1957.

Kalashnikov, N. G., M. N. Pavlovskiy, G. V. Simakov, and R. F. Trunin, Dynamic compressibility of calcite-group minerals, Izv. Earth Physics, No. 2, 23-29, 1973.

Lyzenga, G. A., and T. J. Ahrens, The relation between the shock-induced free-surface velocity and the post-shock specific volume of solids, J. Appl. Phys., 49, 201-204, 1978.

Lyzenga, G. A., T. J. Ahrens, and A. C. Mitchell, Shock temperatures of SiO_2 and their geophysical implications, J. Geophys. Res., 88, 2431-2444, 1983.

Marsh, S. P., LASL Shock Hugoniot Data. Los Angeles, Univ. Cal. Press. 658pp., 1980.

Podurets, M. A., L. V. Popov, A. G. Sevast'yanova, G. V. Simakov, and R. F. Trunin, On the relation between the size of studied specimens and the position of the silica shock adiabat, Izv. Earth Physics, No. 11, 59-60, 1976.

Podurets, M. A., and R. F. Trunin, Unique features in the shock compressibility of silicon dioxide upon manifestation of phase transition kinetics singularities, Comb. Expl. Shock Waves 23, 90-92, 1987.

Rice, M. H., R. G. McQueen, and J. M. Walsh, Compression of solids by strong shock waves, Solid State Phys., 6, 1-63, 1958.

Robie, R. R., B. S. Hemingway, and J. R. Fisher, Thermodynamic Properties of Minerals and Related Substances at 298.15 K and 1 bar (10^5 Pascals) Pressure and at Higher Temperatures, U. S. Geol. Surv. Bull. 1952, 456 pp., 1978.

Salje, E., and K. Viswanathan, The phase diagram calcite-aragonite as derived from the crystallographic properties, Contrib. Mineral. Petrol., 55, 55-67, 1976.

Sekine, T., T. S. Duffy, A. M. Rubin, W. W. Anderson, and T. J. Ahrens, Shock compression and isentropic release of granite, Geophys. J. Int, submitted.

Sumino, Y., and O. L. Anderson, Elastic constants of minerals, in CRC Handbook of Physical Properties of Rocks, vol. III (R. S. Carmichael, ed.), Boca Raton, CRC Press, 39-138, 1984.

Swegle, J. W., Irreversible phase transitions and wave propagation in silicate geologic materials, J. Appl. Phys., 68, 1563-1579, 1990.

Trunin, R. F., G. V. Simakov, and M. A. Podurets, Compression of porous quartz by strong shock waves, Izv. Earth Physics, No. 2, 33-39, 1971a.

Trunin, R. F., G. V. Simakov, M. A. Podurets, B. N. Moiseyev, and L. V. Popov, Dynamic compressibility of quartz and quartzite at high pressure, Izv. Earth Physics, No. 1, 13-20, 1971b.

Tyburczy, J. A., and T. J. Ahrens, Dynamic compression and volatile release of carbonates, J. Geophys. Res., 91, 4730-4744, 1986.

Van Thiel, M., Compendium of Shock Wave Data, Lawrence Livermore Laboratory, UCRL-50108, 1977.

Vizgirda, J., and T. J. Ahrens, Shock compression of aragonite and implications for the equation of state of carbonates, J. Geophys. Res., 87, 4747-4758, 1982.

Wackerle, J., Shock-wave compression of quartz, J. Appl. Phys., 33, 922-937, 1962.